REPORT DOCUMENTATION PAGE

Form Approved OMB No. 0704-0188

1. REPORT DATE *(DD-MM-YYYY)*	2. REPORT TYPE	3. DATES COVERED *(From – To)*
09-10-2008	Final Report	1 July 2007 - 28-Jan-10

4. TITLE AND SUBTITLE

DESIGN OF METAMATERIALS FOR MICROWAVE FREQUENCIES

5a. CONTRACT NUMBER
FA8655-07-1-3039

5b. GRANT NUMBER

5c. PROGRAM ELEMENT NUMBER

6. AUTHOR(S)

Dr. Christos C TRAPALIS

5d. PROJECT NUMBER

5d. TASK NUMBER

5e. WORK UNIT NUMBER

7. PERFORMING ORGANIZATION NAME(S) AND ADDRESS(ES)

NCSR DEMOKRITOS
PATRIARHOU GROGORIOU E' & NEAPOLEOS
Ag. PARASKEVI 153 10
GREECE

8. PERFORMING ORGANIZATION REPORT NUMBER

N/A

9. SPONSORING/MONITORING AGENCY NAME(S) AND ADDRESS(ES)

EOARD
Unit 4515 BOX 14
APO AE 09421

10. SPONSOR/MONITOR'S ACRONYM(S)

11. SPONSOR/MONITOR'S REPORT NUMBER(S)
Grant 07-3039

12. DISTRIBUTION/AVAILABILITY STATEMENT

Approved for public release; distribution is unlimited.

13. SUPPLEMENTARY NOTES

14. ABSTRACT

This report results from a contract tasking NCSR DEMOKRITOS as follows: Negative refractive index materials with simultaneously negative permittivity and permeability are usually constructed from periodic arrays of thin metal wires and split ring resonators. These structures are highly anisotropic, so their isotropic realizations demand three dimensional orthogonal arrangement which are not so easy to fabricate. The aim of this proposal is construction of isotropic homogeneous metamaterial at microwave frequencies that is easy to realize and has possibility of extension to infrared and optical frequencies. The project is organized into three phases with the duration three, six and three months accordingly. In Phase I, (System set up and calibration), the calibration procedures those are required to provide measurements with coaxial line standards and in a free space will we examined. The home made FORTRAN programs will be written to perform TRL (through-reflect-line) calibration procedure in a free space. In Phase II, (Samples preparation and measurement in coaxial line and free space), includes sample preparation and coaxial and free space measurements. Ferroelectric particles from barium titanate and rutile of different sizes (in millimeter and sub-millimeter ranges 0.1-3 mm) and of different volume fractions dispersed in neutral matrix will be used. In Phase III, (Preparation and measurement of final composites), includes analyzing measurement results, samples with suitable sets of particles will be chosen to construct artificial bi-spherical double negative composite.

15. SUBJECT TERMS
EOARD, Left-Handed Materials

16. SECURITY CLASSIFICATION OF:			17. LIMITATION OF ABSTRACT	18, NUMBER OF PAGES	19a. NAME OF RESPONSIBLE PERSON
a. REPORT	b. ABSTRACT	c. THIS PAGE			WYNN SANDERS, Maj, USAF
UNCLAS	UNCLAS	UNCLAS	UL	54	19b. TELEPHONE NUMBER *(Include area code)* +44 (0)1895 616 007

Final Report of EOARD Grant # 073039 (FA8655-07-1-3039)

Title: "DESIGN OF METAMATERIALS FOR MICROWAVE FREQUENCIES"

C. Trapalis
Nanofunctional and Nanocomposite Materials Laboratory
Institute of Materials Science,
NCSR Demokritos
153 10, Ag. Paraskevi Attikis, Greece

Athens 2008

Table of contents

	Page
1. Calibration procedure for coaxial line measurements using new GPC-7 standards. ……...	3
1.1. Description of the calibration procedure with GPC7 standards.……	3
1.2. Comparison of the measurement results after application of the calibration with GPC-7 and K-connector calibration standards.……...	5
2. Development of the calibration technique algorithm and home made Fortran program for measurements in a free space based on 12-term error model.…….	8
3. Short theoretical background on ferri- and ferromagnetic composites with negative permeability. ……..	16
4. Measurement results for magnetic powders measured by coaxial line technique. ……..……..	19
4.1. Results for magnetic powders before annealing. ……..	20
4.2. Results for magnetic powders after annealing. …….……	36
5. Discussion of the results and tasks for further research.…….	49
References ……	53

1. Calibration procedure for coaxial line measurements using new GPC-7 standards.

1.1. Description of the calibration procedure with GPC7 standards.

The calibration procedure based on 12-term error model for coaxial line measurements was already described in our previous report in Chapter 3. In this calibration, K-connector standards (open, short and match) were used. The calibration was applied at the K-ends of the K-GPC7 adapters used as a sample holder. The principal difference of the usage of GPC7 standards is a possibility for application of the calibration procedure directly at the GPC7-ends of the K-GPC7 adapters where samples are inserted during the measurement stage. So, the reference planes are established directly at the GPC7 adapter ends. This improves significantly the calibration and measurement results (see the next Chapter).

In the calibration with GPC7 standards, the three one-port standards (short, open, match) are applied at both GPC7-ends of K-GPC7 adapters of Network Analyzer Port 1 and 2. Zero thru standard is realized by direct connection of two GPC7 adapters' ends together. It should be mentioned that original reference planes used in the calibration procedure appear different from the actual ones at the material interfaces. One should correct the measured S-parameters for appropriate phase shift of the reference planes taking into account only the material thickness.

Fig. 1 shows the experimental set-up for measurements with coaxial line technique performing calibration with GPC7 standards. There, the original reference planes at the GPC7-ends of the K-GPC7 adapters are denoted with numbers 1 and 2. During measurement procedure, sample is inserted inside the GPC7-end of the adapter connected to Port 1 of the Network Analyzer. This implies that the S_{11}, S_{21}, S_{12} parameters need correction for the phase shift of the actual material reference plane 1a that is situated at the front material interface. The 2a actual reference plane at the back material interface does not change and coincides with the original reference plane 2. As a result, the S_{22}-parameter does not need correction. If the measurement sample was inserted at the GPC7-end of Port 2 adapter, the only unchanged parameter would be the S_{11}-parameter.

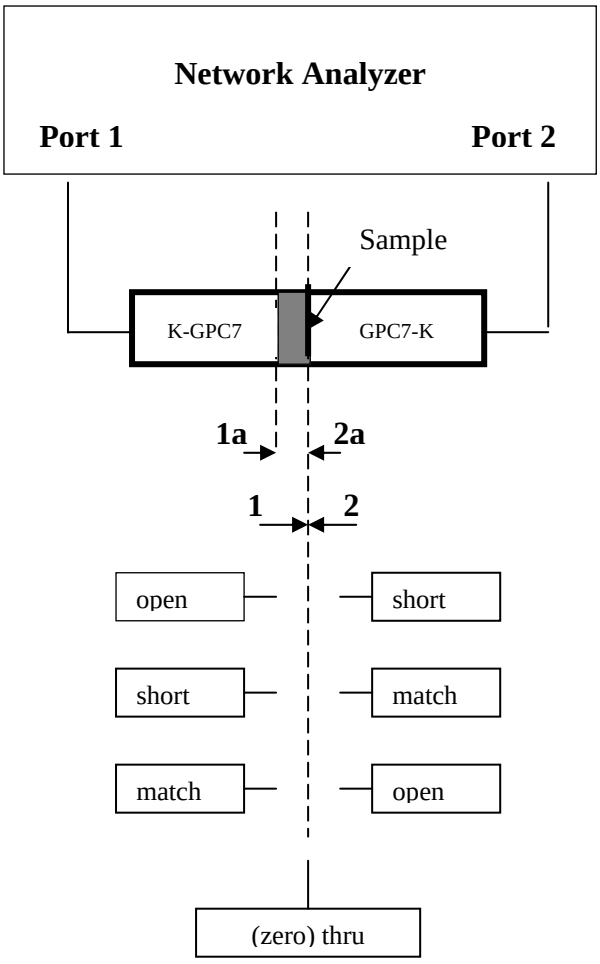

Fig. 1. Experimental setup for S-parameters measurement using coaxial line technique and calibration with GPC7 standards.

Numbers 1 and 2 denote original reference planes used in calibration while numbers 1a and 2a denote actual reference planes at front and back material interfaces, correspondingly. Sample can be inserted inside one of the K-GPC7 adapters. At the figure, sample is inserted in GPC7 adapter of the port 1.

1.2. Comparison of the measurement results after application of the calibration using GPC-7 and K-connector calibration standards.

Fig.2 and Fig. 3 show the measured S-parameters and the retrieved permittivity and permeability of dielectric and magnetic materials that were received with application of two calibrations. In the first calibration (Fig. 2 a, b, c and Fig. 3 a, b, c), the K-connector standards were used. The second case (Figs 2 d, e, f and Fig. 3 d, e, f) relates to calibration that was made with GPC7 standards. To preserve the same calibration conditions, the K-GPC7 adapters that play role of sample holder participated in the calibration procedure not only in the second case where their participation was unavoidable but also in the first case.

The results are presented for barium titanate cubic inclusions (Fig. 2) and cobalt powder (Fig. 3) that were embedded in the inert paraffin matrix. The two kinds of samples represent dielectric and magnetic material, correspondingly. One can perceive from the mentioned figures that usage of K-connector calibration standards in a case of dielectric material can give relatively satisfied results for the permittivity and permeability behavior. The mean value of permittivity is preserved and the sharp dielectric resonance is not distorted. Also, the small relaxation peaks appearing in the permeability spectrum at ~10 GHz as well as at ~17 GHz (Fig 2c) are proved also by measurements after calibration with GPC7 standards (Fig. 2f).

The situation in a case of magnetic material is different. The permeability appears to be more sensitive to the uncorrected S-parameters' oscillations that appear to be more pronounced in these materials. Because of the resonance behavior of the permeability in the GHz frequency range, the mentioned oscillations can shadow real resonances or can give false resonance peaks making measurements of magnetic material permeability fully inapplicable with the usage of K calibration standards.

To observe real permeability characteristics of magnetic materials, calibration with GPC7 standards is needed. For this reason, the new Calibration Kit 6352 was purchased and measurements of magnetic materials after calibration with these standards were realized.

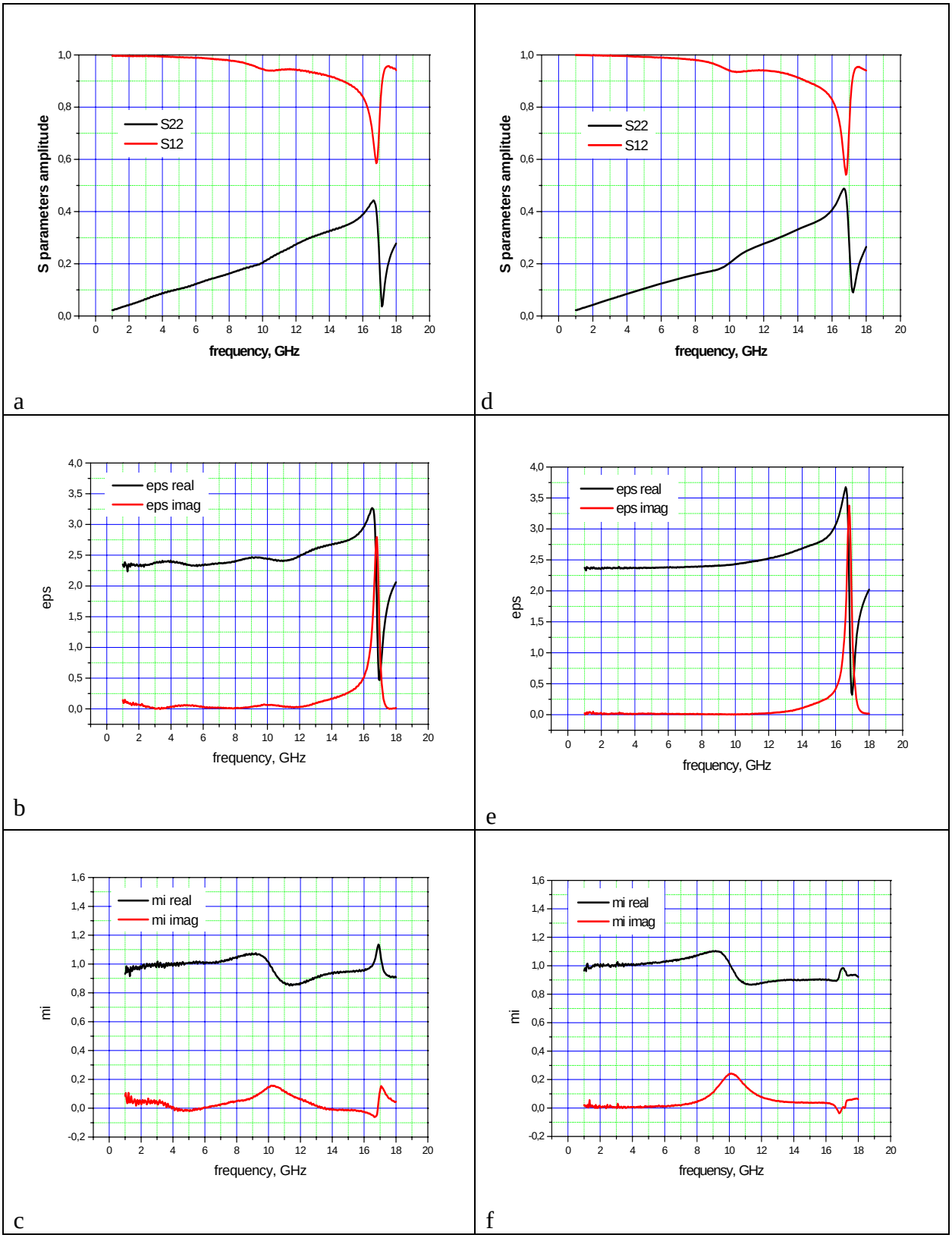

Fig. 2. Experimental results - S parameters and retrieved permittivity and permeability - for B1-12 sample (1 peace of barium titanate embedded in paraffin matrix) via calibration with K-connector standards (a, b, c) and GPC7 standards (d, e, f).

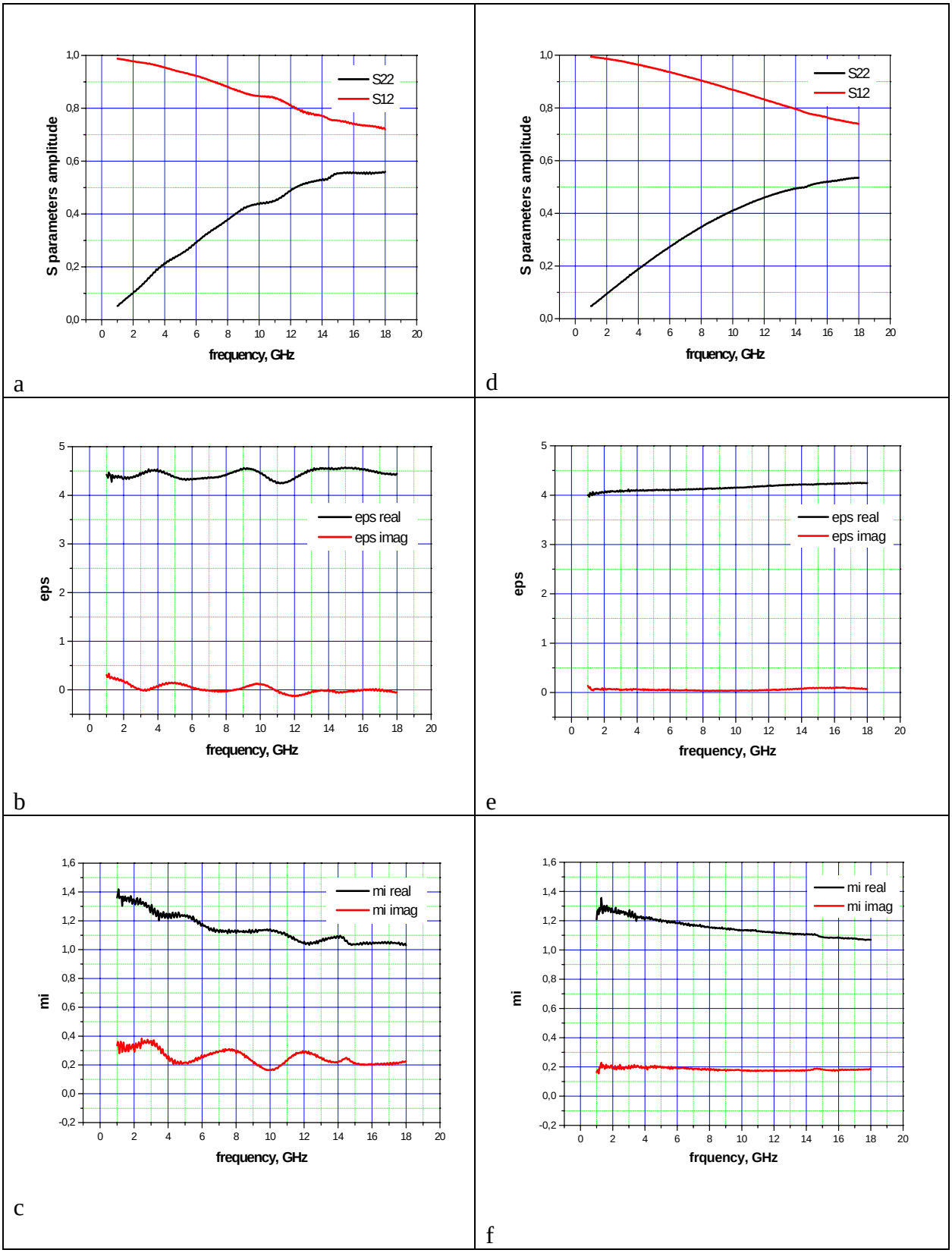

Fig. 3. Experimental results - S parameters and retrieved permittivity and permeability - for C60 sample (Co particles embedded in paraffin matrix with 60 wt%) via calibration with K-connector standards (a, b, c) and GPC7 standards (d, e, f).

2. Development of the calibration technique algorithm and home made Fortran program for measurements in a free space based on 12-term error model.

Free space methods are non-destructive and contactless methods. They are especially suitable for measurement of complex electric permittivity and complex magnetic permeability of the planar objects. There are no restrictions on fabrication of samples with specific shape, for example, in form of toroid as in coaxial line measurements.

Due to systematic errors as e. g. transmission losses of the cables or mismatches of the antennas, a calibration of measurement set-up is necessary. In this chapter we will concern standard full two port 12-term calibration algorithm in application to free space measurements. It should be mentioned that one needs to develop his own software program for performing calibration in a free space in contrast to coaxial line calibration that is realized using ready software that is already “sewed” into commercial Network Analyzers.

In general, measurement of the scattering S-parameters of an unknown device under the test (DUT) should be corrected for repeatable system errors through a system calibration. Any microwave calibration technique must be capable of representing repeatable system errors and provide a method for correcting uncalibrated measurements. Most methods represent these errors by the scattering response of a hypothetical virtual error adapter which interfaces the Network Analyzer to the DUT (Fig. 4). The error terms of the virtual error adapters are computed from the measurement of known standards. Then, the `true' parameters of the DUT can be calculated using these error terms and the measured scattering response of the DUT. The different calibration techniques differ mainly in the proposed error model that is solved and the number and type of standards used. In general, at least three standards are needed for calibration of a two-port device.

In a case of two-port Network Analyzer, the virtual error adapter is a four-port. It has 16 error terms. This follows from the fact that the number of error terms is the square of the number of virtual adapter ports [1].

Many practical systems in coaxial, waveguide and free space do not use all 16 error terms. Currently in industry the full-two-port 12-term or 10-term error models are used which does not include all the leakage and coupling terms [1-5]. In our project we will concern 12-term error model.

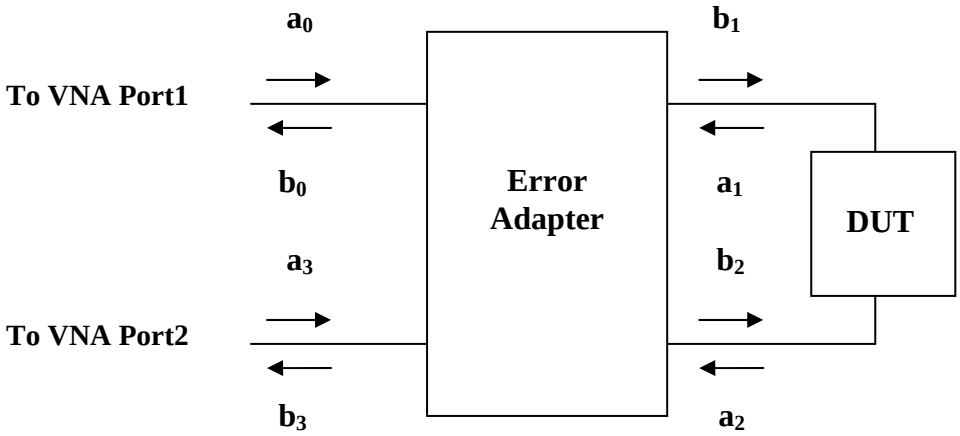

Fig. 4. Error adapter model.

The measured S-parameters connect input signal amplitudes a_0 and a_3 in forward and reverse directions with correspondent output signal amplitudes b_0 and b_3 at the Vector Network Analyzer Port1 and Port2. The actual measured S-parameters connect input signal amplitudes b_1 and b_2 in forward and reverse directions with correspondent output signal amplitudes a_1 and a_2 at the DUT ports. The error model enable to relate actual S-parameters with measured S-parameters of the DUT in terms of error coefficients of the virtual error adapter as is explained in the text.

Let us represent the incoming and the outcoming wave amplitudes at corresponding two ports of the DUT and of the Network Analyzer through the scattering actual and measured S-parameters of the DUT (Fig.4):

$$\begin{bmatrix} a_1 \\ a_2 \end{bmatrix} = S_A \begin{bmatrix} b_1 \\ b_2 \end{bmatrix}; \qquad \begin{bmatrix} b_0 \\ b_3 \end{bmatrix} = S_M \begin{bmatrix} a_0 \\ a_3 \end{bmatrix}; \qquad S_{A,M} = \begin{bmatrix} S_{11A,M} & S_{12A,M} \\ S_{21A,M} & S_{22A,M} \end{bmatrix}. \quad (1)$$

These wave amplitudes can also be written through the error terms of the virtual error adapter in the following way:

$$\begin{bmatrix} b_0 \\ b_3 \\ b_1 \\ b_2 \end{bmatrix} = E \begin{bmatrix} a_0 \\ a_3 \\ a_1 \\ a_2 \end{bmatrix}; \qquad E = \begin{bmatrix} E_1 & E_2 \\ E_3 & E_4 \end{bmatrix}; \qquad (2)$$

where

$$E_1 = \begin{bmatrix} e_{00} & e_{03} \\ e_{30} & e_{33} \end{bmatrix}; \qquad E_2 = \begin{bmatrix} e_{01} & e_{02} \\ e_{31} & e_{32} \end{bmatrix}; \qquad E_3 = \begin{bmatrix} e_{10} & e_{13} \\ e_{20} & e_{23} \end{bmatrix}; \qquad E_4 = \begin{bmatrix} e_{11} & e_{12} \\ e_{21} & e_{22} \end{bmatrix}. \quad (3)$$

The Eq. (2) can be rewritten in the form:

$$\begin{bmatrix} b_0 \\ b_3 \end{bmatrix} = E_1 \begin{bmatrix} a_0 \\ a_3 \end{bmatrix} + E_2 \begin{bmatrix} a_1 \\ a_2 \end{bmatrix}; \qquad \begin{bmatrix} b_1 \\ b_2 \end{bmatrix} = E_3 \begin{bmatrix} a_0 \\ a_3 \end{bmatrix} + E_4 \begin{bmatrix} a_1 \\ a_2 \end{bmatrix}. \qquad (4)$$

By using linear algebra, solutions for the actual and measured S-parameters of the unknown DUT in terms of the error adapter can be obtained:

$$S_A = \left[E_3((S_M - E_1)^{-1} E_2 + E_4)\right]^{-1} \qquad (5a)$$

$$S_M = E_1 + E_2 S_A (1 - E_4 S_A)^{-1} E_3 \qquad (5b)$$

The 12-error model accounts for the following error terms containing six terms in forward direction and six terms in reverse direction. The 6 terms of the forward direction are:

e_{00} - forward directivity,

e_{11}- port1 match in forward direction,

e_{22} - port 2 match in forward direction,

e_{10} e_{01} - forward reflection tracking,

e_{10} e_{32} - forward transmission tracking,

e_{30} -forward isolation

The six terms of the reverse direction are:

e'_{33} - forward directivity,

e'_{22}- port1 match in forward direction,

e'_{11} - port 2 match in forward direction,

e'_{32} e'_{23} - forward reflection tracking,

e'_{23} e'_{01} - forward transmission tracking,

e'_{03} -forward isolation.

The expansion of the Eqs. (5a) taking into account only the mentioned 12 error terms leads to the following expressions for calculation of the actual S-parameters:

$$S_{11A} = \frac{\left(\frac{S_{11M} - e_{00}}{e_{10}e_{01}}\right)\left(1 + \frac{S_{22M} - e'_{33}}{e'_{23}e'_{32}}e'_{22}\right) - e_{22}\left(\frac{S_{21M} - e_{30}}{e_{10}e_{32}}\right)\left(\frac{S_{12M} - e'_{03}}{e'_{23}e'_{01}}\right)}{\Delta}; \quad (6a)$$

$$S_{21A} = \frac{\left(\frac{S_{21M} - e_{30}}{e_{10}e_{32}}\right)\left[1 + \left(\frac{S_{22M} - e'_{33}}{e'_{23}e'_{32}}\right)\left(e'_{22} - e_{22}\right)\right]}{\Delta}; \quad (6b)$$

$$S_{12A} = \frac{\left(\frac{S_{12M} - e'_{03}}{e'_{23}e'_{01}}\right)\left[1 + \left(\frac{S_{11M} - e_{00}}{e_{10}e_{01}}\right)\left(e_{11} - e'_{11}\right)\right]}{\Delta} \quad (6c)$$

$$S_{22A} = \frac{\left(\frac{S_{22M} - e'_{33}}{e'_{23}e'_{32}}\right)\left(1 + \frac{S_{11M} - e_{00}}{e_{10}e_{01}}e_{11}\right) - e'_{11}\left(\frac{S_{21M} - e_{30}}{e_{10}e_{32}}\right)\left(\frac{S_{12M} - e'_{03}}{e'_{23}e'_{01}}\right)}{\Delta} \quad (6d)$$

where

$$\Delta = \left(1 + \frac{S_{11M} - e_{00}}{e_{10}e_{01}}e_{11}\right)\left(1 + \frac{S_{22M} - e'_{33}}{e'_{23}e'_{32}}\right) - e_{22}e'_{11}\left(\frac{S_{21M} - e_{30}}{e_{10}e_{32}}\right)\left(\frac{S_{12M} - e'_{03}}{e'_{23}e'_{01}}\right) \quad (6e)$$

Also, the expansion of the Eqs. (5b) leads to the following expressions for calculation of the measured S-parameters depending on the mentioned 12 error terms:

$$S_{11M} = e_{00} + e_{10}e_{01}\frac{S_{11A} - e_{22}\Delta_{SA}}{\Delta'}; \qquad (7a)$$

$$S_{21M} = e_{30} + e_{10}e_{32}\frac{S_{21A}}{\Delta'}; \qquad (7b)$$

$$S_{12M} = e'_{03} + e'_{23}e'_{01}\frac{S_{12A}}{\Delta''}; \qquad (7c)$$

$$S_{22M} = e'_{33} + e'_{23}e'_{32}\frac{S_{22A} - e'_{11}\Delta_{SA}}{\Delta''}. \qquad (7d)$$

Here: $\Delta_{SA} = S_{11A}S_{22A} - S_{21A}S_{12A};$

$$\Delta' = 1 - e_{11}S_{11A} - e_{22}S_{22A} + e_{11}e_{22}\Delta_{SA}; \qquad (7e)$$

$$\Delta'' = 1 - e'_{11}S_{11A} - e'_{22}S_{22A} + e'_{11}e'_{22}\Delta_{SA}.$$

The 12 error terms can be determined using one-port standards and thru connection using the Eqs (7) The three one-port standards for measurements in a free space can be a short (metal plate at horn aperture), an open (metal plate at some distance from horn aperture) and a match (open horn) standards. If the one-port standards are connected to Port 1 in the forward direction Eq. (7a) becomes:

$$S_{11M} = e_{00} + e_{10}e_{01}\frac{S_{11A}}{1 - e_{11}S_{11A}}; \qquad (8)$$

This equation can be written as a bilinear transform:

$$S_{11M} = \frac{aS_{11A} + b}{cS_{11A} + 1}, \qquad (9)$$

and also can be written in the linear form:

$$aS_{11A} + b - cS_{11A}S_{11M} - S_{11M} = 0, \qquad (10)$$

where

$$\begin{aligned} a &= e_{10}e_{01} - e_{00}e_{11}, \\ b &= e_{00}, \\ c &= -e_{11} \end{aligned} \qquad (11)$$

With three known one-port standards, three independent equations can be written:

$$\begin{aligned} &aS_{11A1} + b - cS_{11A1}S_{11M1} - S_{11M1} = 0; \\ &aS_{11A2} + b - cS_{11A2}S_{11M2} - S_{11M2} = 0; \\ &aS_{11A3} + b - cS_{11A3}S_{11M3} - S_{11M3} = 0. \end{aligned} \qquad (12)$$

The above three linear equations can be solved for three unknowns a, b and c:

$$a = \frac{\det\begin{bmatrix} S_{11M1} & 1 & -S_{11A1}S_{11M1} \\ S_{11M2} & 1 & -S_{11A2}S_{11M2} \\ S_{11M3} & 1 & -S_{11A3}S_{11M3} \end{bmatrix}}{\det A} \qquad (13a)$$

$$b = \frac{\det\begin{bmatrix} S_{11A1} & S_{11M1} & -S_{11A1}S_{11M1} \\ S_{11A2} & S_{11M2} & -S_{11A2}S_{11M2} \\ S_{11A3} & S_{11M3} & -S_{11A3}S_{11M3} \end{bmatrix}}{\det A} \qquad (13b)$$

$$c = \frac{\det\begin{bmatrix} S_{11A1} & 1 & S_{11M1} \\ S_{11A2} & 1 & S_{11M2} \\ S_{11A3} & 1 & S_{11M3} \end{bmatrix}}{\det A} \qquad (13c)$$

There:

$$\det A = \det\begin{bmatrix} S_{11A1} & 1 & -S_{11A1}S_{11M1} \\ S_{11A2} & 1 & -S_{11A2}S_{11M2} \\ S_{11A3} & 1 & -S_{11A3}S_{11M3} \end{bmatrix}. \qquad (13d)$$

These a, b and c coefficients can give e_{00}, e_{11} and $e_{10}e_{01}$ error terms:

$$e_{00} = b, \quad e_{11} = -c \quad \text{and} \quad e_{10}e_{01} = a - bc. \qquad (14)$$

With match standard applied at Port 1 and Port 2 the isolation term e_{30} can be determined directly from the Eq. (7b):

$$S_{21M4} = e_{30}. \qquad (15)$$

With thru connection (Port 1 and Port 2 are joined together) Eq. (7a) can be written:

$$S_{11M5} = e_{00} + e_{10}e_{01}\frac{e_{22}}{1 - e_{11}e_{22}} \qquad (16)$$

and can be solved for e_{22}:

$$e_{22} = \frac{S_{11M5} - e_{00}}{(S_{11M5} - e_{00})e_{11} + e_{10}e_{01}}. \qquad (17)$$

With thru connection Eq. (7b) can be written:

$$S_{21M6} = e_{30} + e_{10}e_{32}\frac{1}{1 - e_{11}e_{22}} \qquad (18)$$

and can be solved for $e_{10}e_{32}$:

$$e_{10}e_{32} = \frac{S_{21M\,6} - e_{30}}{1 - e_{11}e_{22}}. \qquad (19)$$

This way, the six forward error terms are determined and the same procedure can be used for the six error terms in the reverse direction.

Analogously, application of three one-port standards at Port 2 can give three equations for determination e'_{33}, e'_{22} and $e'_{23}e'_{32}$. The Eq. (7d) can be reduced to:

$$S_{22M} = e'_{33} + e'_{23}e'_{32}\frac{S_{22A}}{1 - e'_{22}S_{22A}}, \qquad (20)$$

and then written in the linear form giving following three equation with three unknowns a', b' and c':

$$\begin{aligned} &a'S_{22A1} + b' - c'S_{22A1}S_{22M1} - S_{22M1} = 0; \\ &a'S_{22A2} + b' - c'S_{22A2}S_{22M2} - S_{22M2} = 0; \\ &a'S_{22A3} + b' - c'S_{22A3}S_{22M3} - S_{22M3} = 0. \end{aligned} \qquad (21)$$

These three unknowns give the three error terms:

$$e'_{33} = b', \quad e'_{22} = -c' \quad \text{and} \quad e'_{23}e'_{32} = a' - b'c'. \qquad (22)$$

Then, with match standard at Port1 and Port2, the isolation term e'_{03} can be determined directly from the Eq. (7c):

$$S_{12M4} = e'_{03}. \qquad (23)$$

With the thru connection, Eq. (7d) is reduced to:

$$S_{22M5} = e'_{33} + e'_{23}e'_{32}\frac{e'_{11}}{1 - e'_{11}e'_{22}}. \qquad (24)$$

Then the expression for error e'_{11} term is easily derived:

$$e'_{11} = \frac{S_{22M5} - e'_{33}}{(S_{22M5} - e'_{33})e'_{22} + e'_{23}e'_{32}}. \qquad (25)$$

With thru connection, Eq. (7c) is reduced:

$$S_{12M6} = e'_{03} + e'_{23}e'_{01}\frac{1}{1 - e'_{11}e'_{22}}. \qquad (26)$$

It gives the expression for error $e'_{23}e'_{01}$ term:

$$e'_{23}e'_{01} = \frac{S_{12M6} - e'_{03}}{1 - e'_{11}e'_{22}} . \qquad (27)$$

Now, all 12 error terms in forward and reverse directions are known. They can be used for determination of actual S-parameters of the DUT from its measured S-parameters through the Eqs. (6).

The algorithm described above that gives equations for determination of error coefficients was used in writing home-made Fortran programs for providing free space calibration and material actual S-parameters calculation.

3. Short theoretical background on ferri- and ferromagnetic composites with negative permeability.

In the recent years, complex permeability spectra of composite ferri- and ferromagnetic materials in the microwave frequency range became a subject of considerable interest in the viewpoint of the applications to the new field of left handed materials. A possibility to realize negative permeability spectra required as one of the necessary properties for the left handed materials is considered in [6-9]. Here [6], frequency dispersion of permeability in an yttrium–iron–garnet (YIG) under external magnetic field is investigated. Through examining the compositional dependence of the magnetic properties of the synthesized $BaFe_{12-x}(Ti_{0.5}Co_{0.5})_xO_{19}$ substituted hexaferrite, the compositional region of appearing the negative permeability spectra in the GHz frequency region without external field is discussed in [7]. Also, negative permeability is reported in ferromagnetic metal granular composites composed of permalloys and Co powders in the vicinity of the natural resonance frequencies [8, 9]. Based on the effective medium approximation, paper [10] shows that by incorporating metallic magnetic nanoparticles into an appropriate insulating matrix and controlling the directions of magnetization of metallic magnetic components and their volume fraction, it may be possible to prepare a composite medium of low eddy current loss that is left-handed for electromagnetic waves propagating in some special direction and polarization in a frequency region near the ferromagnetic resonance frequency.

It is assumed that a permeability dispersion of the ferrite and ferromagnetic metal composites usually consists of two different magnetizing mechanisms: domain wall motion resonance and spin rotational resonance (also, natural spin or gyromagnetic spin resonance) [11].

The domain wall resonance is affected by grain size of magnetic inclusions while the gyromagnetic spin resonance in absence of the external magnetic field occurs in the internal magnetic field produced by the crystalline magnetic anisotropy.

The simple frequency dispersion formula can be written containing two components owing to domain-wall and gyromagnetic spin motion [11]:

$$\mu = 1 + \chi_{dw} + \chi_{sp} = 1 + \frac{\omega_{dw}^2 K_{dw}}{\omega_{dw}^2 + \omega + i\omega\beta} + \frac{(\omega_{sp} + i\omega\alpha)\omega_{sp} K_{sp}}{(\omega_{sp} + i\omega\alpha)^2 - \omega^2} \ . \qquad (28)$$

There, χ_{dw} and χ_{sp} are magnetic susceptibility for domain-wall and gyromagnetic spin motions, ω_{dw} and ω_{sp} are resonance frequencies of domain-wall and spin components, K_{dw} and K_{sp} are the static magnetic susceptibility of each component, α and β are damping factors, and ω is the frequency of external electromagnetic fields. In this formula, if α is large enough ($\alpha \to \infty$) the χ_{sp} can be approximated by the relaxation-type frequency dispersion:

$$\mu = 1 + \frac{\omega_{dw}^2 K_{dw}}{\omega_{dw}^2 + \omega + i\omega\beta} + \frac{K_{sp}}{1 + i\dfrac{\omega}{\omega_{sp}}} \qquad (29)$$

Therefore, relaxation type magnetization rotation can be estimated by the high value of damping factor α in formula (28).

In the most of the known spinel and hexaferrites, the relaxation type of spin gyromagnetic motion takes place. This leads to broadened permeability spectra with no negative values of the real part of the permeability near the spin resonance frequency.

However, it is not in a case with the substituted Ba ferrites $BaFe_{12-x}(Ti_{0.5}Co_{0.5})_xO_{19}$ as is reported in [7]. Since the domain wall resonance in these ferrites takes place in a relatively low frequency region up to several 100 MHz, observed permeability spectra in several GHz is considered to be mainly attributed to the gyromagentic spin resonance. In $BaFe_9(Ti_{0.5}Co_{0.5})_3O_{19}$ (x=3), the negative permeability dispersion of permeability in zero external magnetic field can be seen above 2 GHz. This result indicates that this substituted barium ferrite is a good candidate for the negative permeability part of a left-handed materials.

It was shown [8, 9] that a heat-treatment of ferromagnetic metal particles is effective to suppress the eddy current effect in the complex permeability spectra of some permalloy and single metal composite materials. Negative permeability in the permalloy $Ni_{45}Fe_{55}$ (mean particle size 2.53 μm) and $Ni_{47}Fe_{53}$ (mean particle size 6 μm) and in the cobalt (mean particle size 45 μm) composites with high particle content was observed in the microwave frequency range.

If the particle content of ferromagnetic metallic composite material embedded in inert matrix is higher than the percolation limit of the particles, the mechanical contact among the embedded particles is established in this composite material. In a case of the non heat-treated composite, Ohmic contact of the percolated particles brings about the metallic conductivity of the composite. The frequency dispersion of the imaginary part of permittivity shows abrupt increase. However, in the heat-treated particle composite materials, non-Ohmic contact among

the particles accompanies with high electrical resistivity and insulating properties can be maintained even in the high particle content. Accordingly, the eddy current in the composite is suppressed and natural resonance owing to the internal magnetic anisotropy field in the particles can be seen in the permeability spectra.

Probably, the damping of gyromagnetic spin resonance which mainly contributes to permeability in the high frequency range is smaller in permalloy composites than that in spinel ferrite composites. In addition, the spin resonance frequency of permalloy composites is higher than that in spinel ferrite composites. Thus, the resonance-type frequency dispersion of permeability accompanying with negative permeability can be obtained in the insulating state in permalloy composite materials without the eddy current effect.

The permeability of 79 vol.% cobalt and 67 vol.% $Ni_{47}Fe_{53}$ composites become zero around 6 GHz. The 70 vol.% $Ni_{45}Fe_{55}$ composite has a negative permeability at over 5GHz [8, 9]. Thus, ferromagnetic metal composite materials containing the heat-treated particles can be a candidate for left handed materials.

4. Measurement results for magnetic powders measured by coaxial line technique

The following ferromagnetic powders were purchased from Alfa Aesar:

1) 10255 Ni powder, 100g, particle size 2-3 μm;

2) 00170 Fe powder, 250g, paticle size < 10 μm;

3) 10455 Co powder, 100g, particle size 1.6 μm;

4) 36683 Fe-Ni powder (50%-50%), 100g, 325 mesh (< 44 μm);

5) 44600 Fe-Ni powder (65%-35%), 100g, 325 mesh (< 44 μm).

The powders were mixed in different weight fractions with paraffin. Samples in a form of toroid with inside and outside diameters d_{in}= 3.04 mm and d_{out}=7.00 mm, correspondingly, to suit GPC7 coaxial adapters were prepared with the help of special moulds. In the Table I, we show the powders with their weight fractions that were used for sample preparation. The weight fraction of the powder is marked by two digit numbers after the letter designating each powder. The following designations were used for the powders: Ni powder - N, Fe powder - F, Co powder - C, Fe-Ni (50-50) - FN, Fe-Ni (65-35) - FNX.

Table I. List of the samples prepared from the powders before annealing.

C60	N60	F60	FN60	FNX60
C70	N70	-	FN70	-
C80	N80	-	FN80	-
C90	N90	F80	FN90	FNX90

In the Table II, we reference the samples with correspondent volume fractions that were prepared after annealing of the powders (the letter “H” is assigned to annealing (heat-treating) of the powders).

Table II. List of the samples prepared from the powders after annealing.

300^{o}C, 5 hours				
CH80	NH80	FH80	FNH80	FNXH80
CH90	NH90	FH90	FNH90	FNXH90
400^{o}C, 3 hours				
-	NH490-3	-	FNH490-3	-
400^{o}C, 6 hours				
-	NH490-6	-	-	-

4.1. Results for magnetic powders before annealing

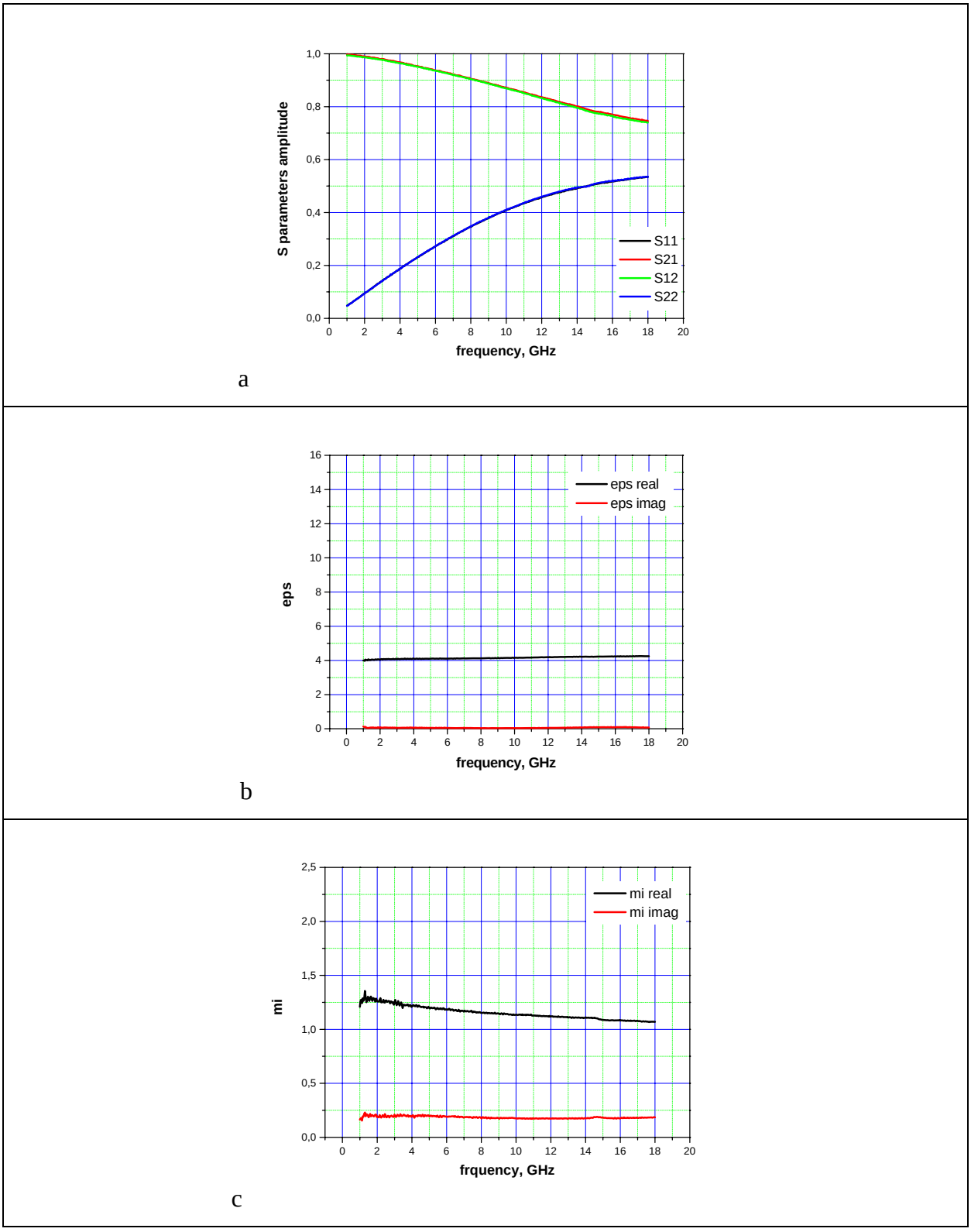

Fig. 5. Measured S-parameters and retrieved permittivity and permeability for sample C60 (60 %wt Co powder in paraffin matrix, 1.64 mm ring thickness).

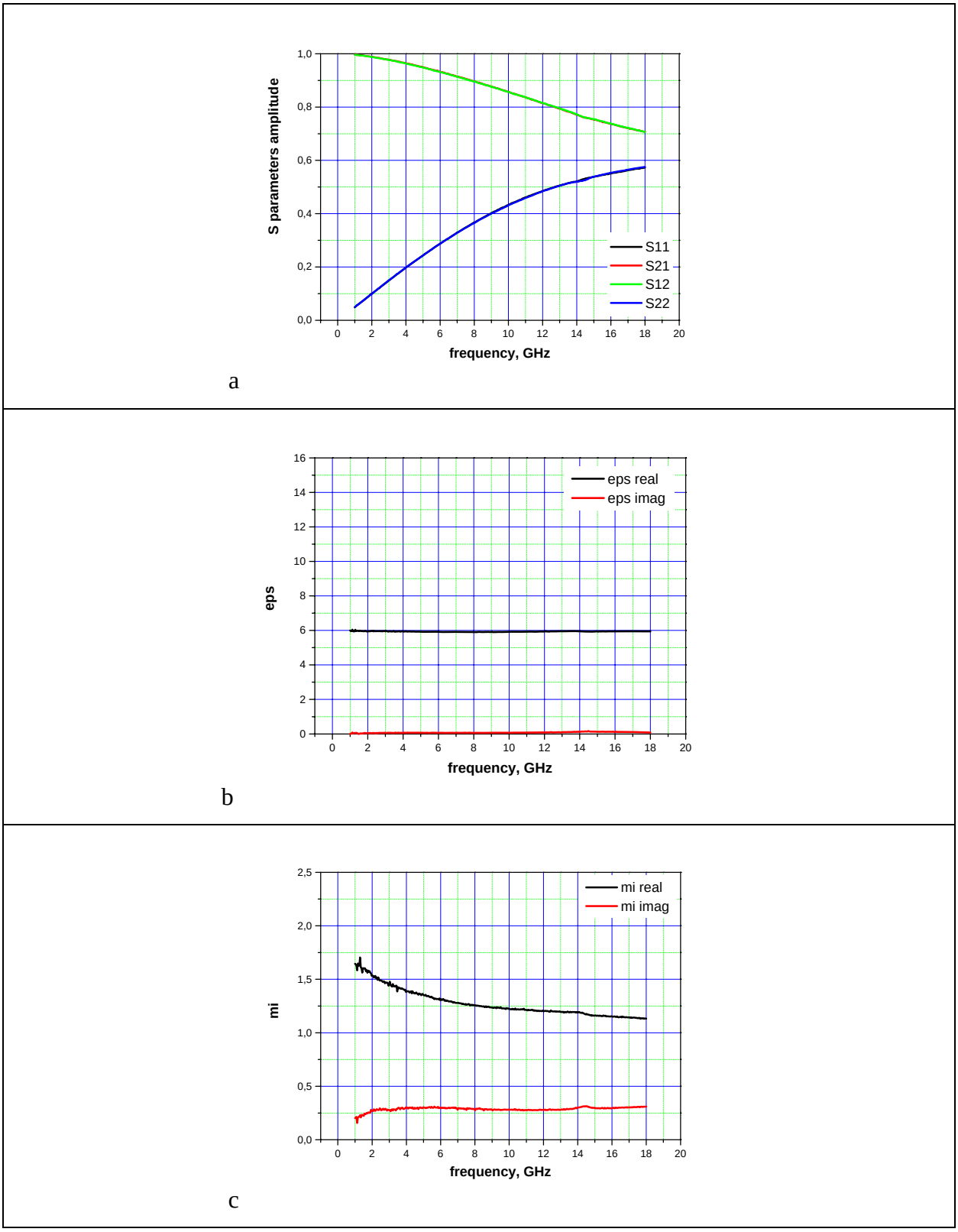

Fig. 6. Measured S-parameters and retrieved permittivity and permeability for sample C70 (70 %wt Co powder in paraffin matrix, 1.09 mm ring thickness).

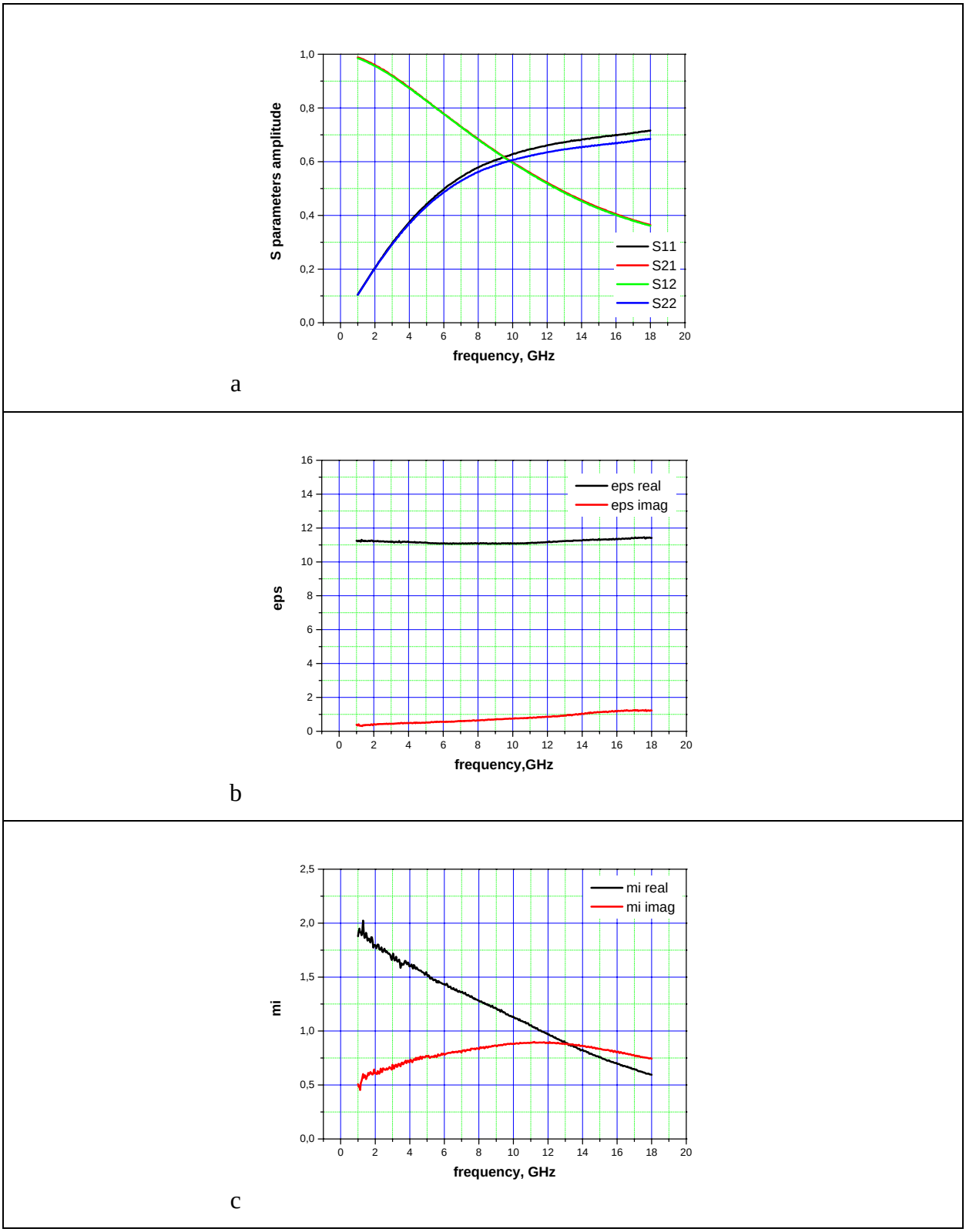

Fig. 7. Measured S-parameters and retrieved permittivity and permeability for sample C80 (80 %wt Co powder in paraffin matrix, 1.08 mm ring thickness).

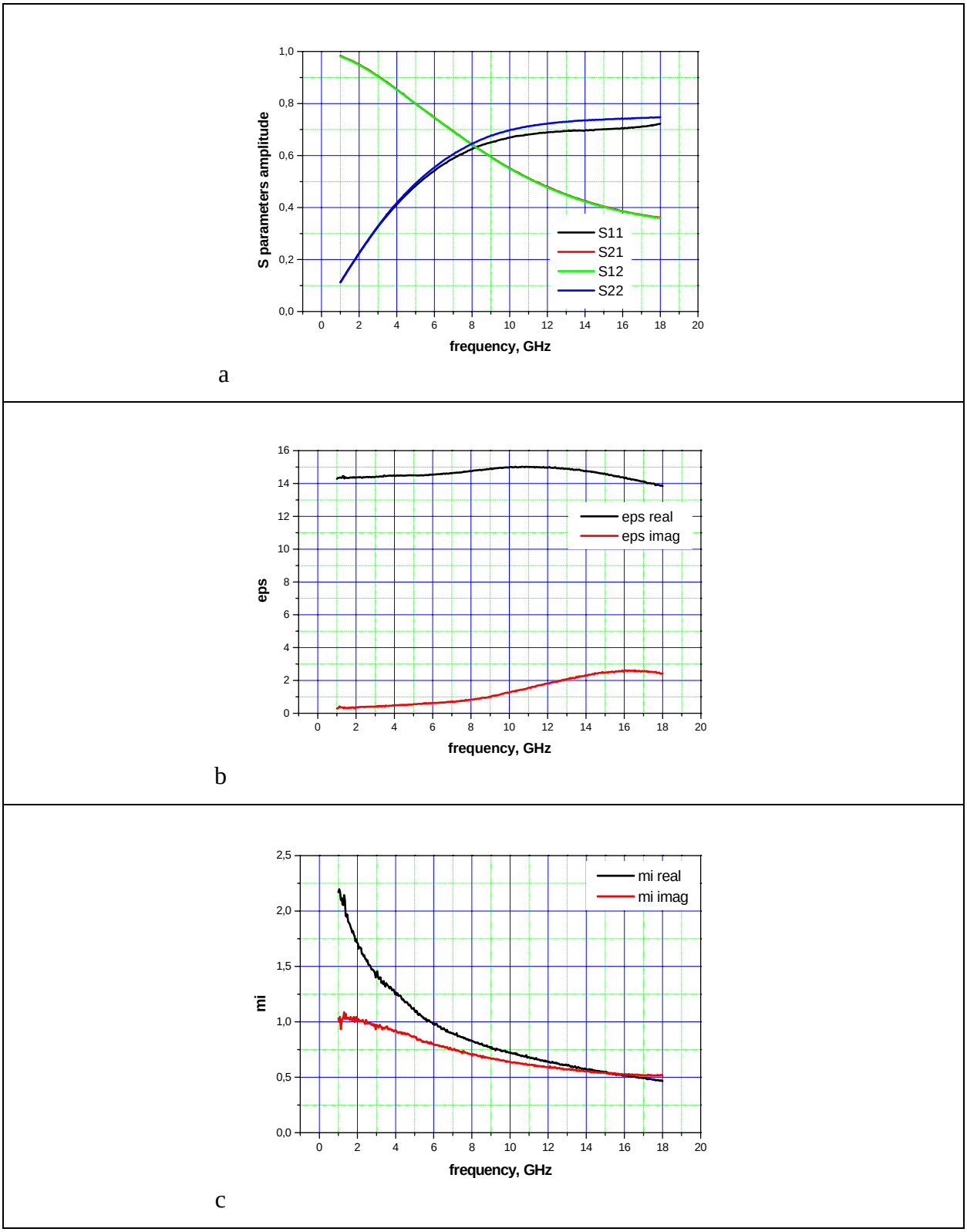

Fig. 8. Measured S-parameters and retrieved permittivity and permeability for sample C90 (90 %wt Co powder in paraffin matrix, 0.90 mm ring thickness).

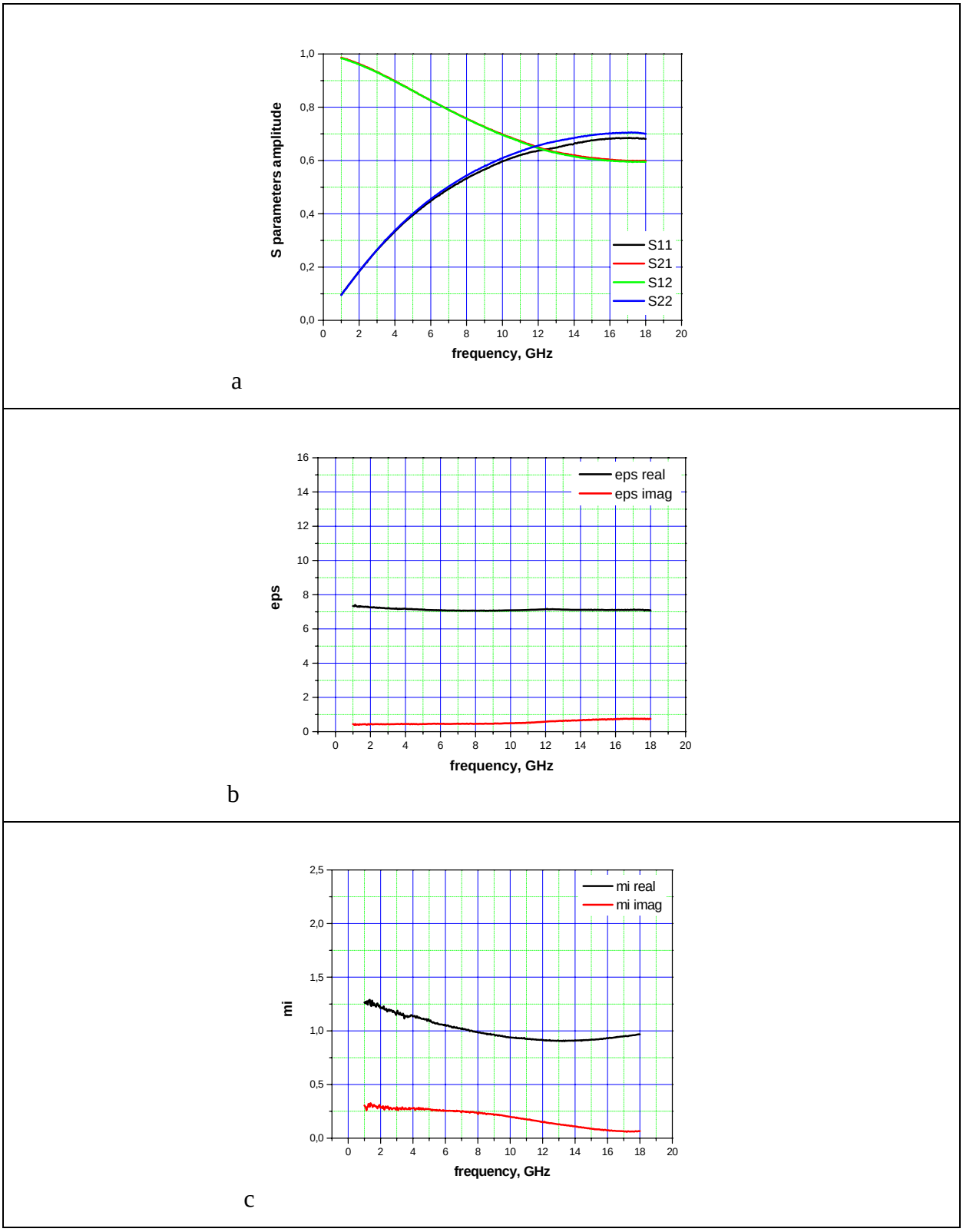

Fig. 9. Measured S-parameters and retrieved permittivity and permeability for sample N60 (60 %wt Ni powder in paraffin matrix, 1.52 mm ring thickness).

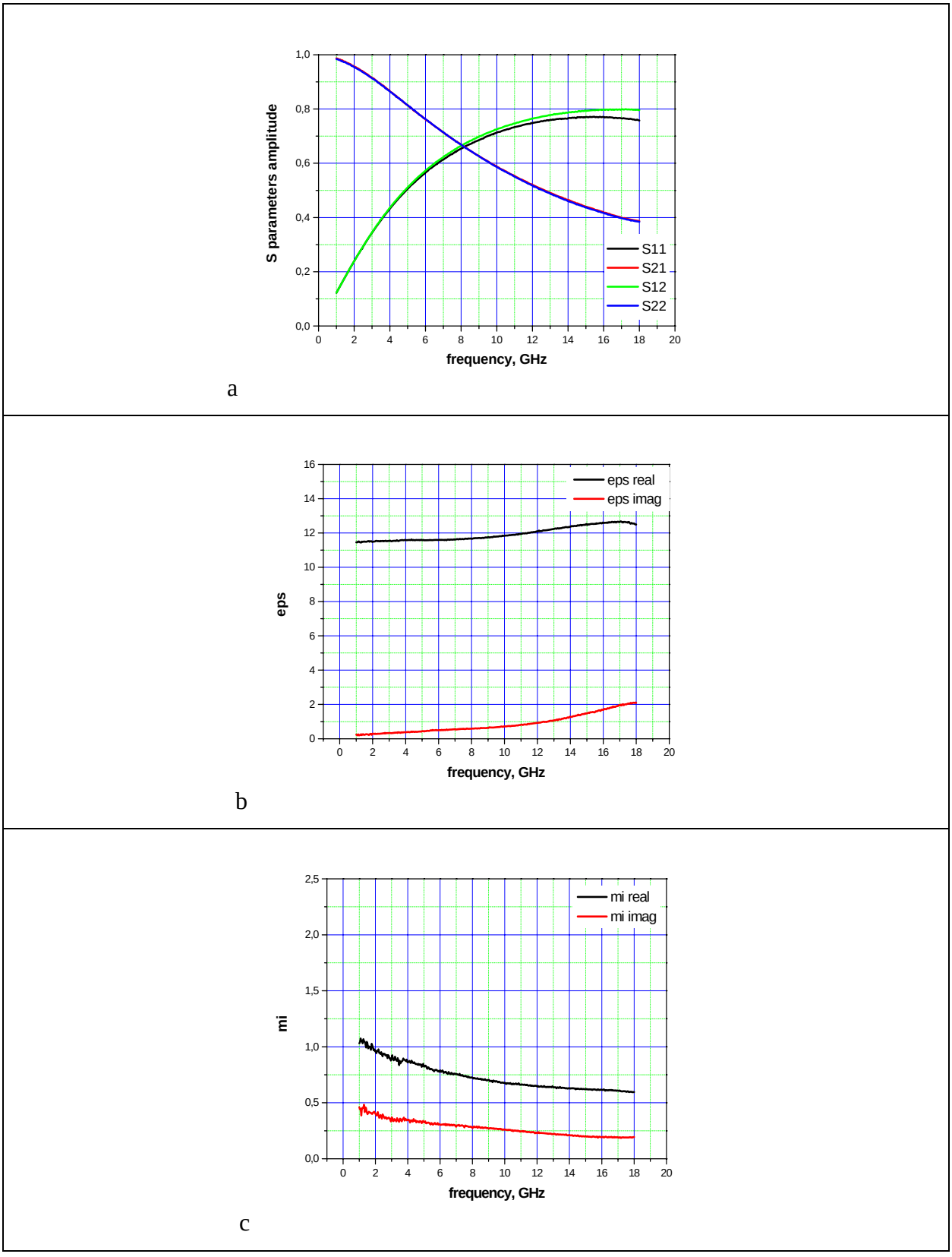

Fig. 10. Measured S-parameters and retrieved permittivity and permeability for sample N70 (70 %wt Ni powder in paraffin matrix, 1.14 mm ring thickness).

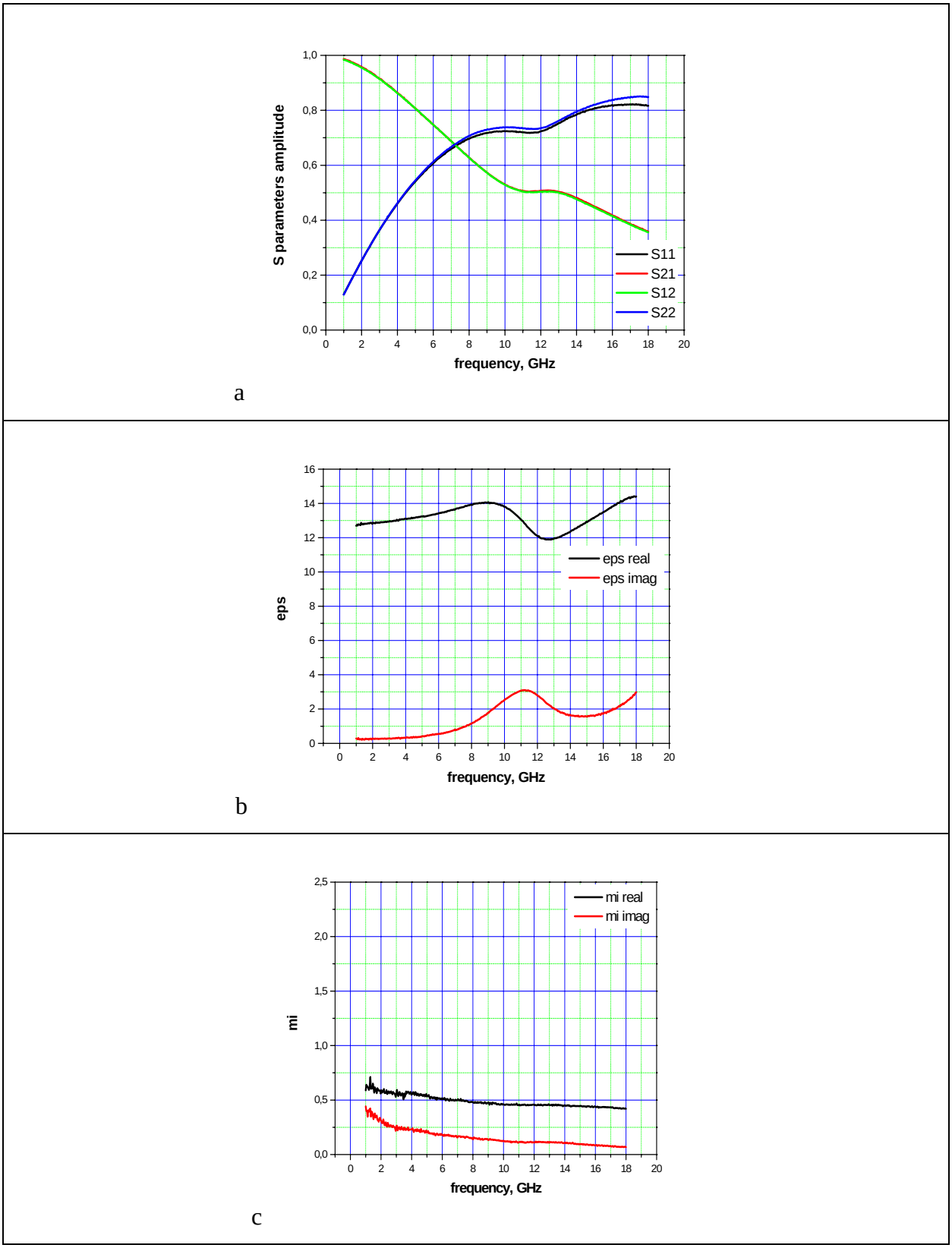

Fig. 11. Measured S-parameters and retrieved permittivity and permeability for sample N80 (80 %wt Ni powder in paraffin matrix, 1.03 mm ring thickness).

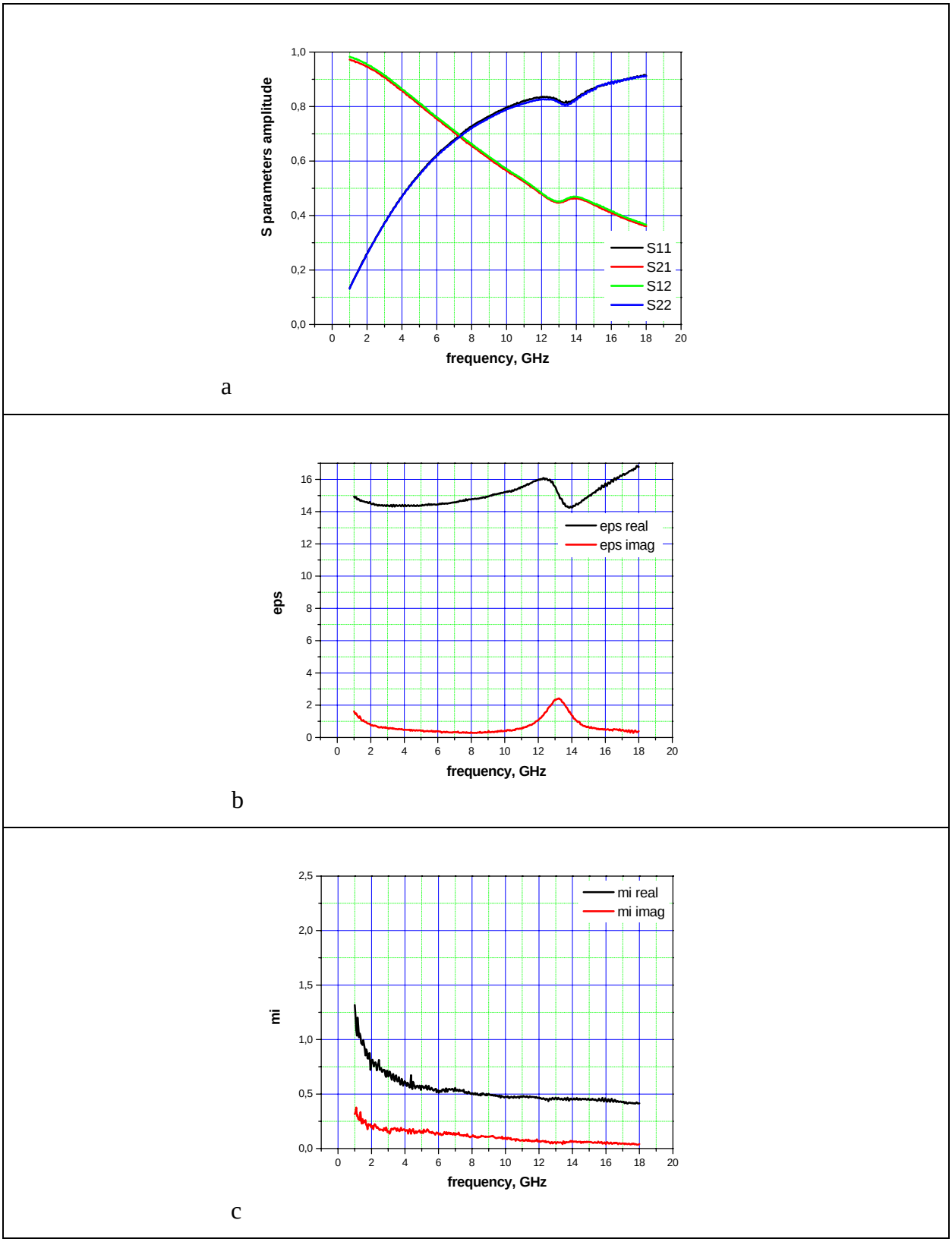

Fig. 12. Measured S-parameters and retrieved permittivity and permeability for sample N90 (90 %wt Ni powder in paraffin matrix, 0.96 mm ring thickness).

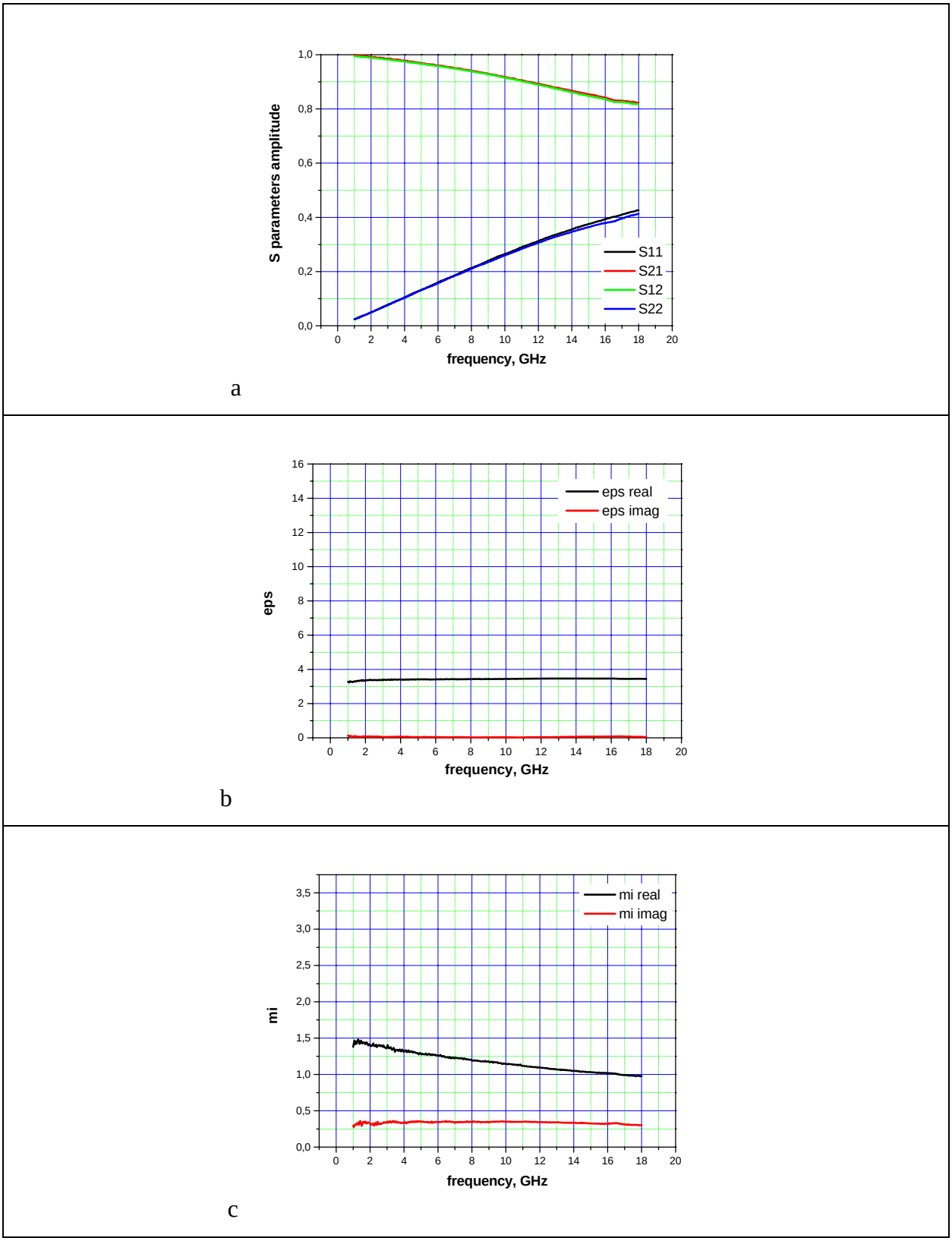

Fig. 13. Measured S-parameters and retrieved permittivity and permeability for sample F60 (60 %wt Fe powder in paraffin matrix, 1.22 mm ring thickness).

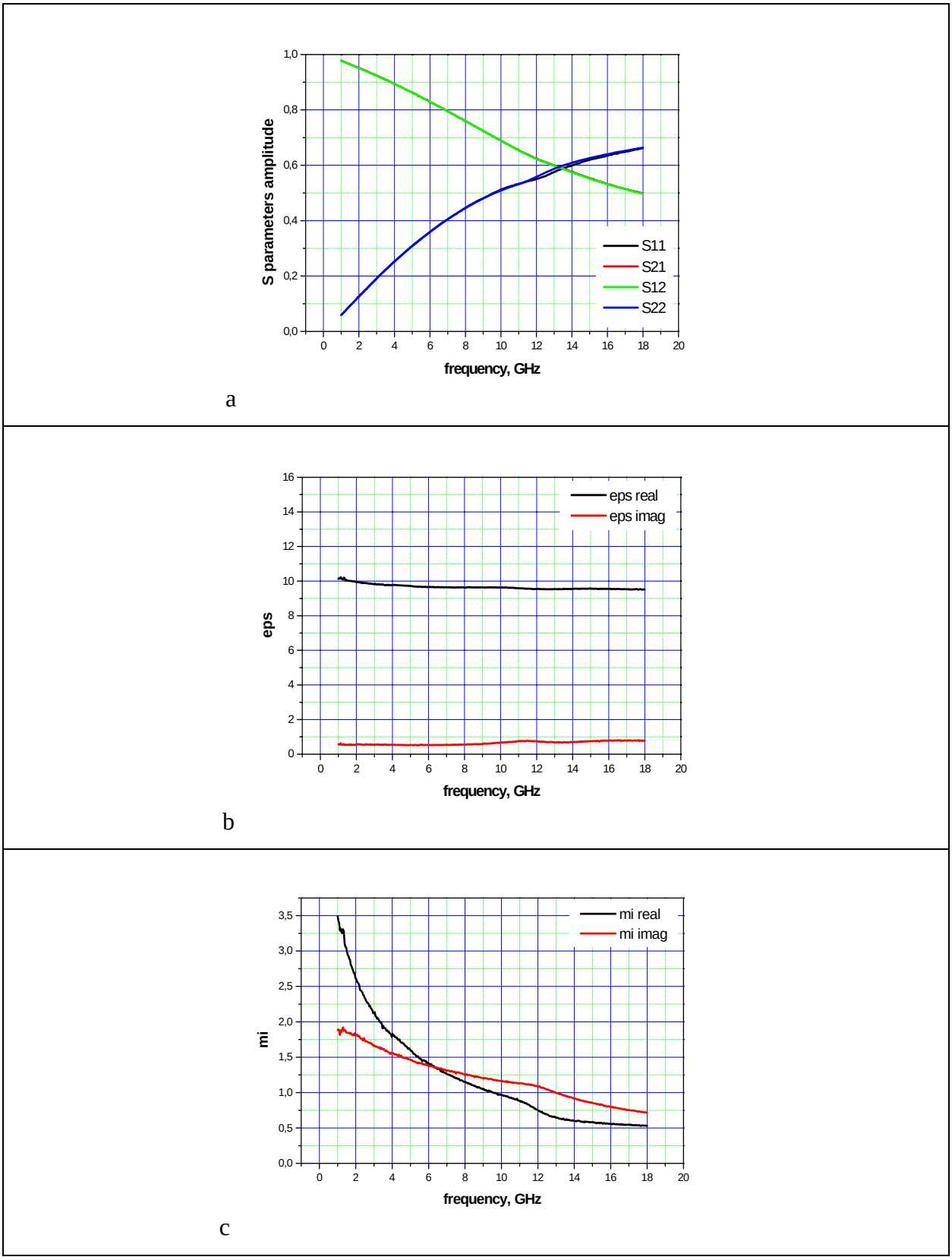

Fig. 14. Measured S-parameters and retrieved permittivity and permeability for sample F90 (90 %wt Fe powder in paraffin matrix, 1.22 mm ring thickness).

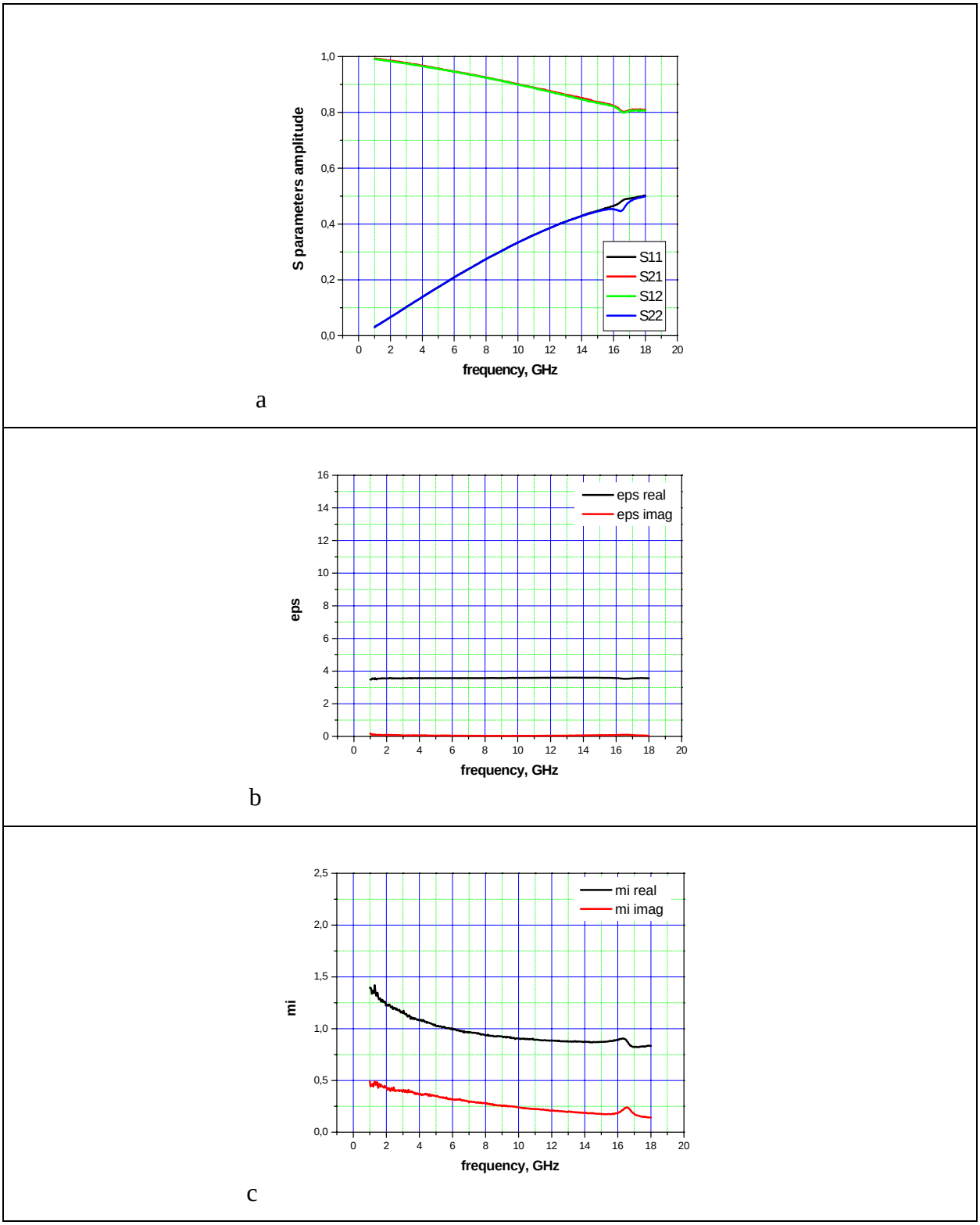

Fig. 15. Measured S-parameters and retrieved permittivity and permeability for sample FN60 (60 %wt Fe-Ni (50%-50%) powder in paraffin matrix, 1.38 mm ring thickness).

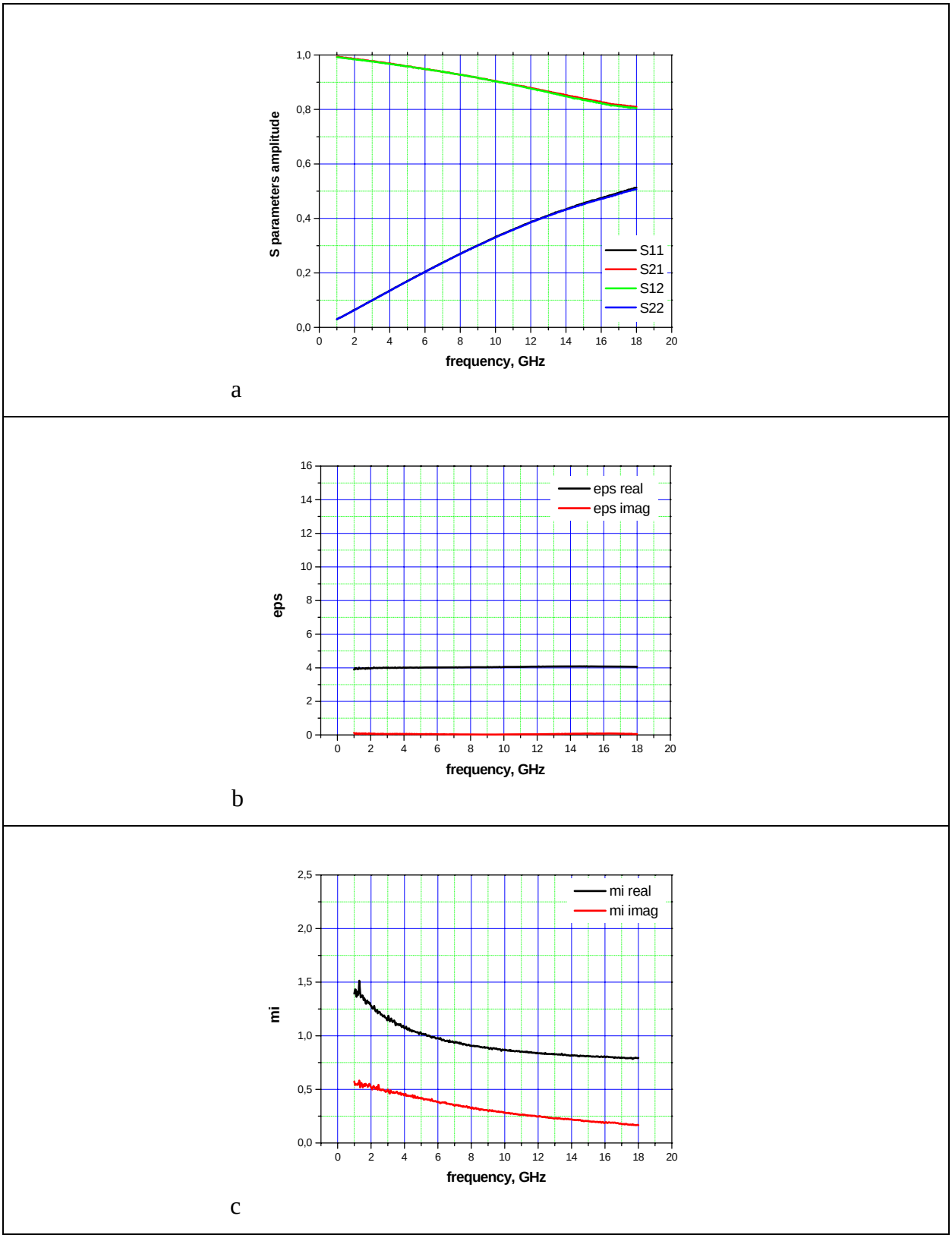

Fig. 16. Measured S-parameters and retrieved permittivity and permeability for sample FN70 (70 %wt Fe-Ni (50%-50%) powder in paraffin matrix, 1.13 mm ring thickness).

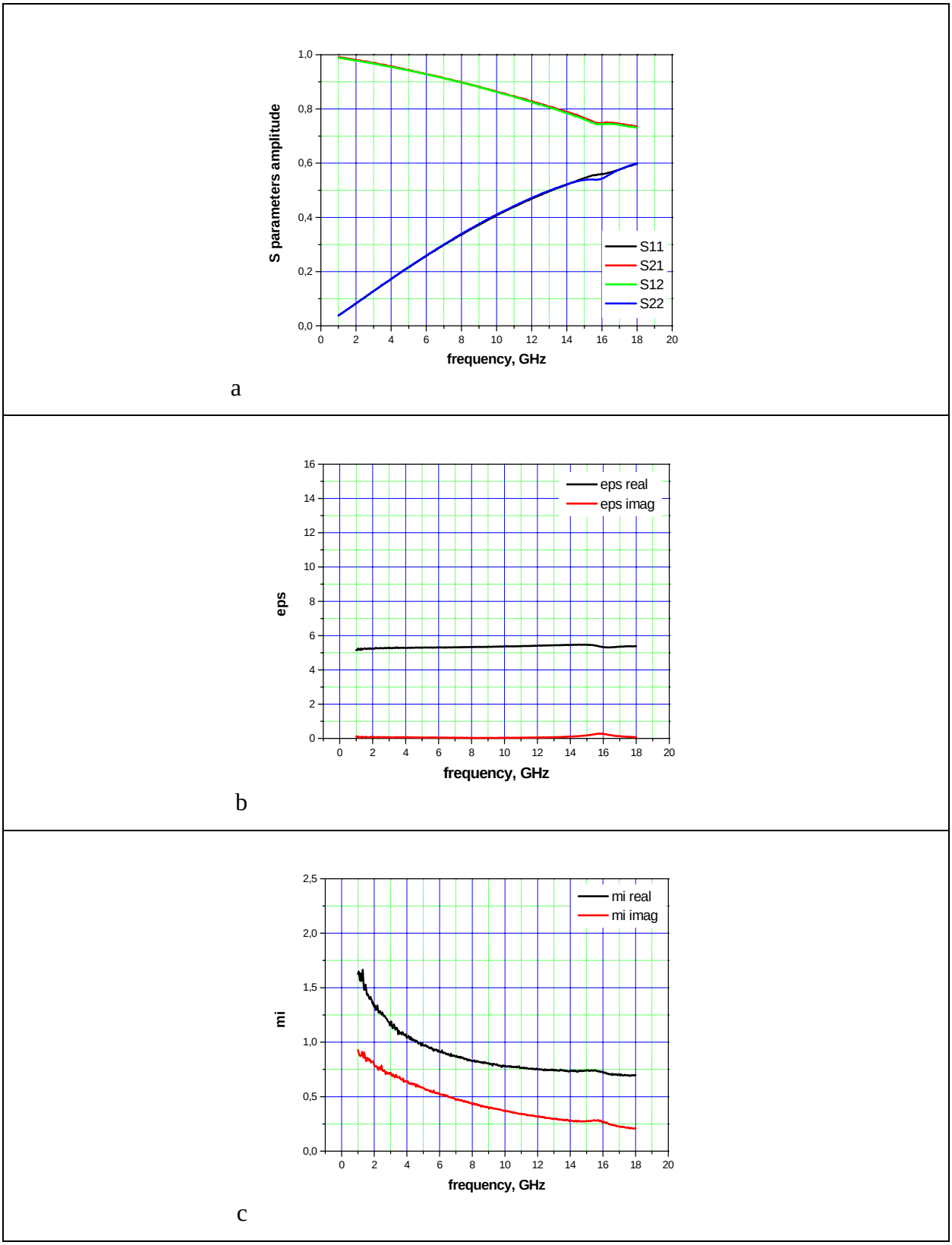

Fig. 17. Measured S-parameters and retrieved permittivity and permeability for sample FN80 (80 %wt Fe-Ni (50%-50%) powder in paraffin matrix, 1.02 mm ring thickness).

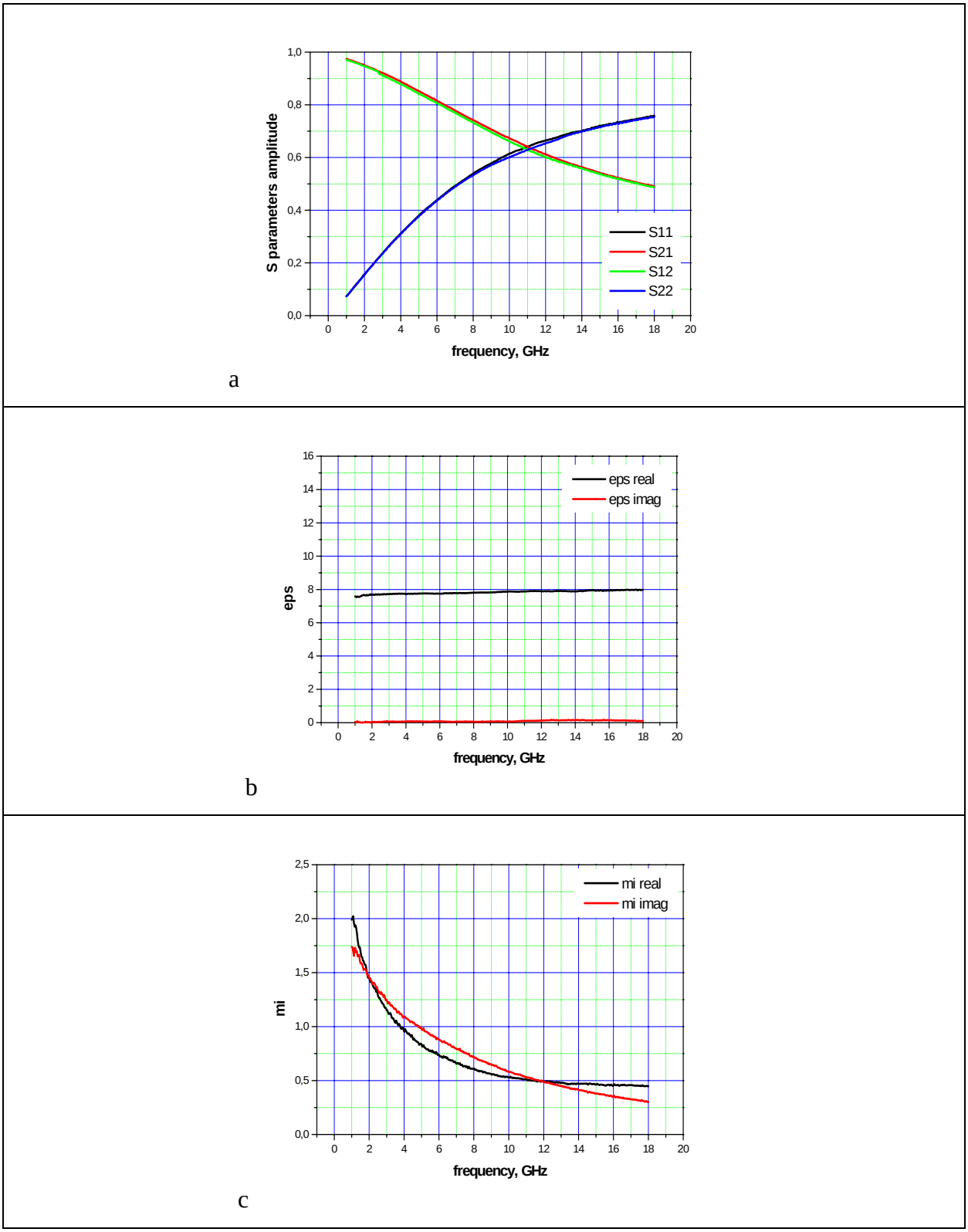

Fig. 18. Measured S-parameters and retrieved permittivity and permeability for sample FN90 (90 %wt Fe-Ni (50%-50%) powder in paraffin matrix, 1.24 mm ring thickness).

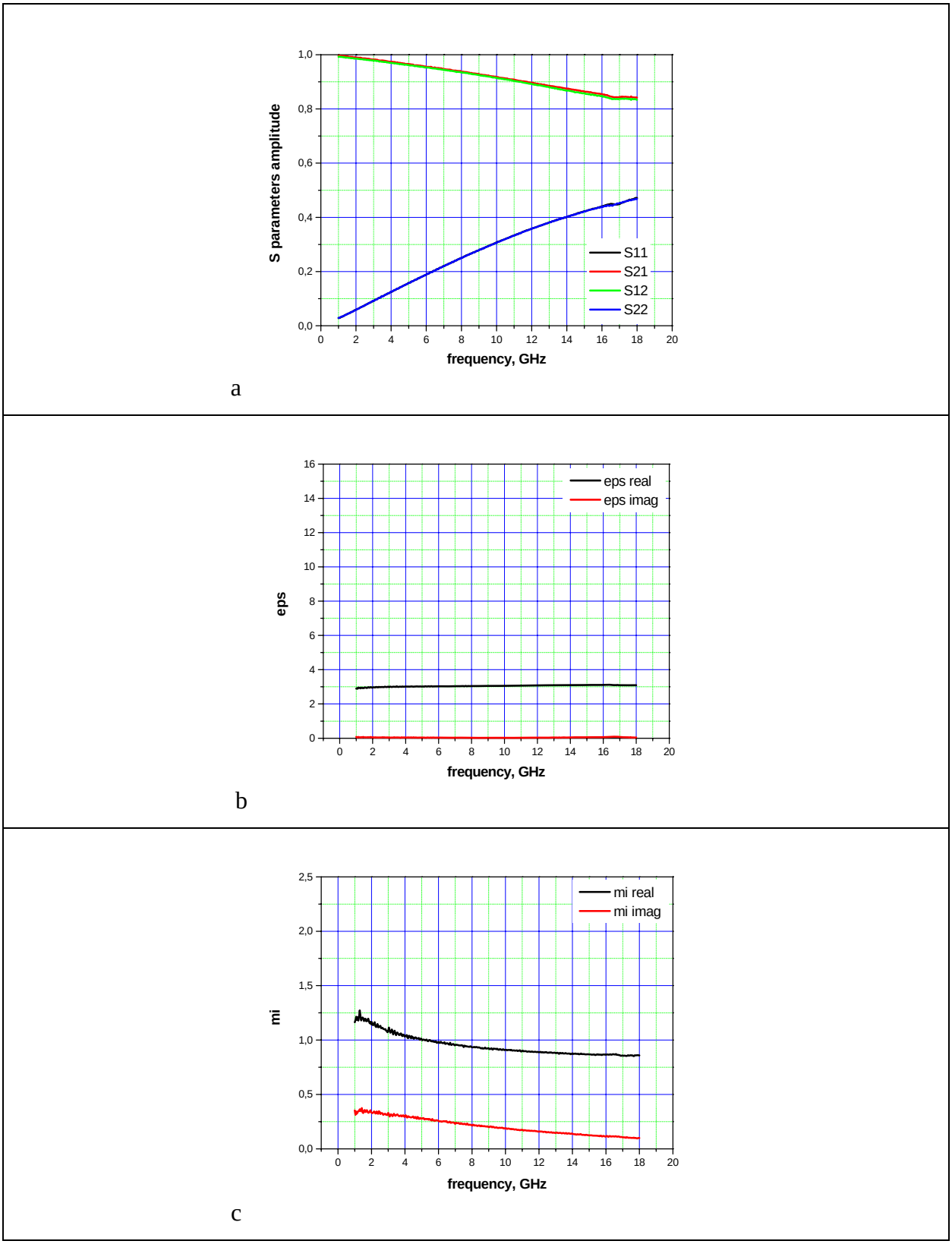

Fig. 19. Measured S-parameters and retrieved permittivity and permeability for sample FNX60 (60 %wt Fe-Ni (65%-35%) powder in paraffin matrix, 1.56 mm ring thickness).

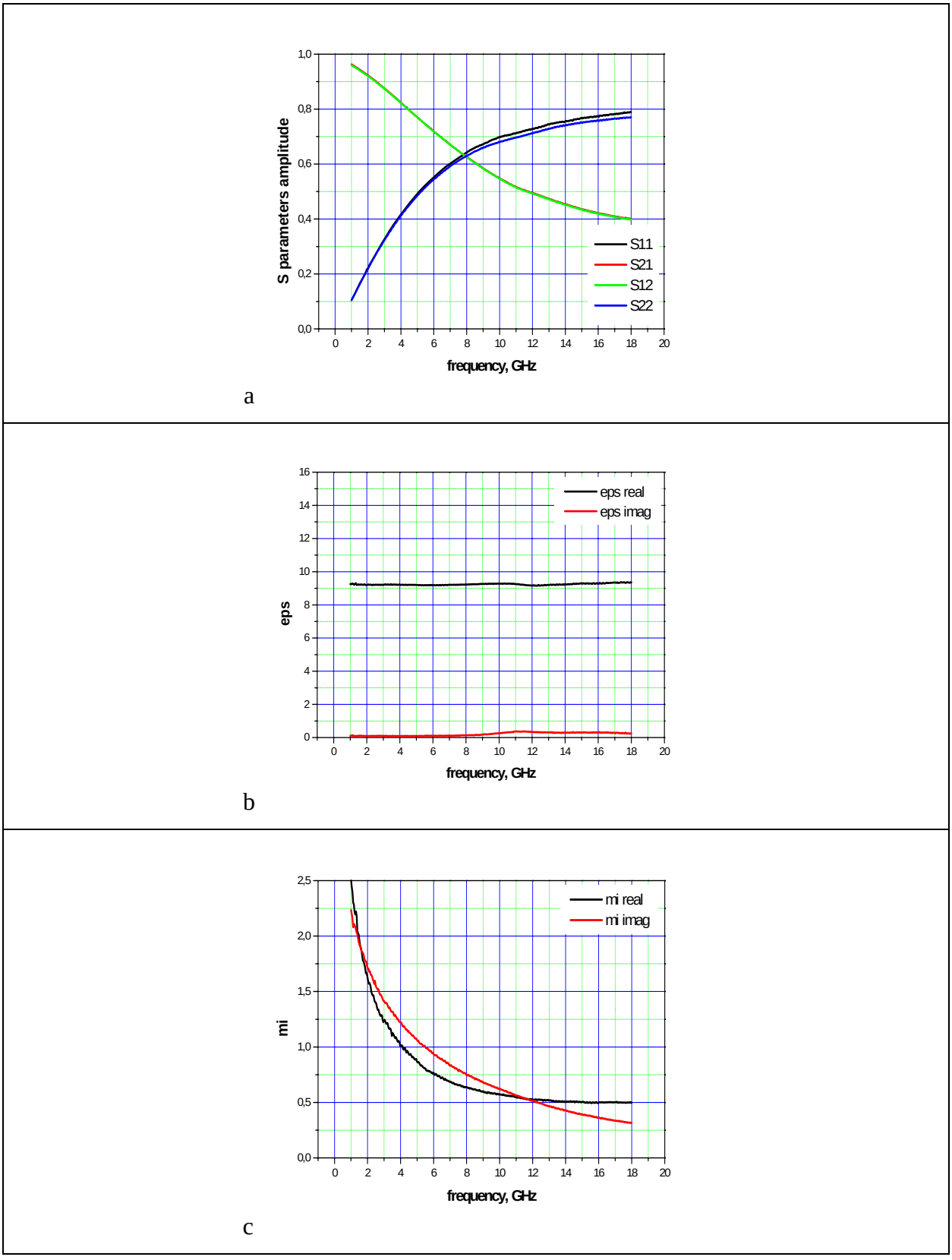

Fig. 20. Measured S-parameters and retrieved permittivity and permeability for sample FNX90 (90 %wt Fe-Ni (65%-35%) powder in paraffin matrix, 1.48 mm ring thickness).

4.2. Results for magnetic powders after annealing.

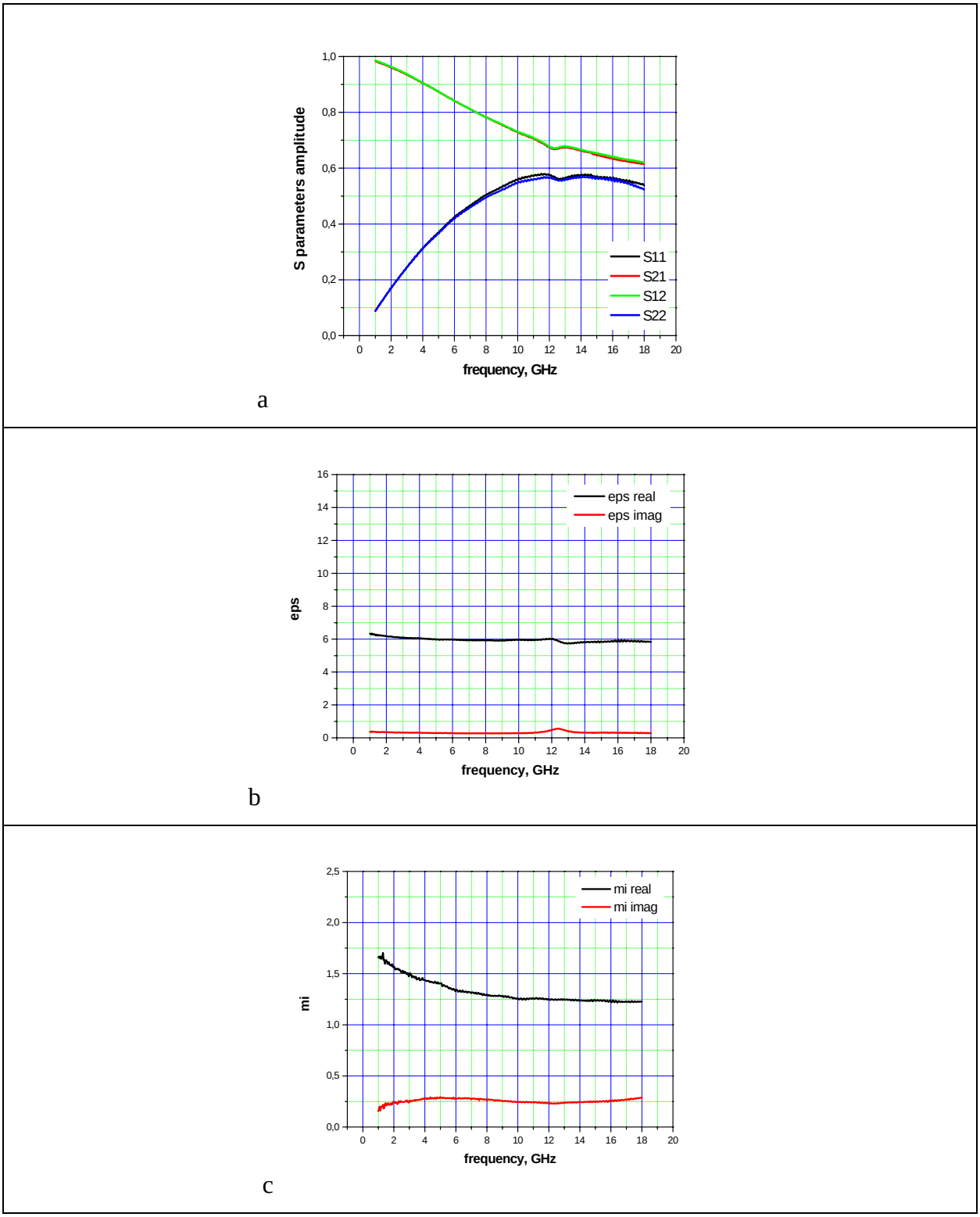

Fig. 21. Measured S-parameters and retrieved permittivity and permeability for sample CH80 (80 %wt Co powder in paraffin matrix annealed at 300^{o}C 5h, 1.84 mm ring thickness).

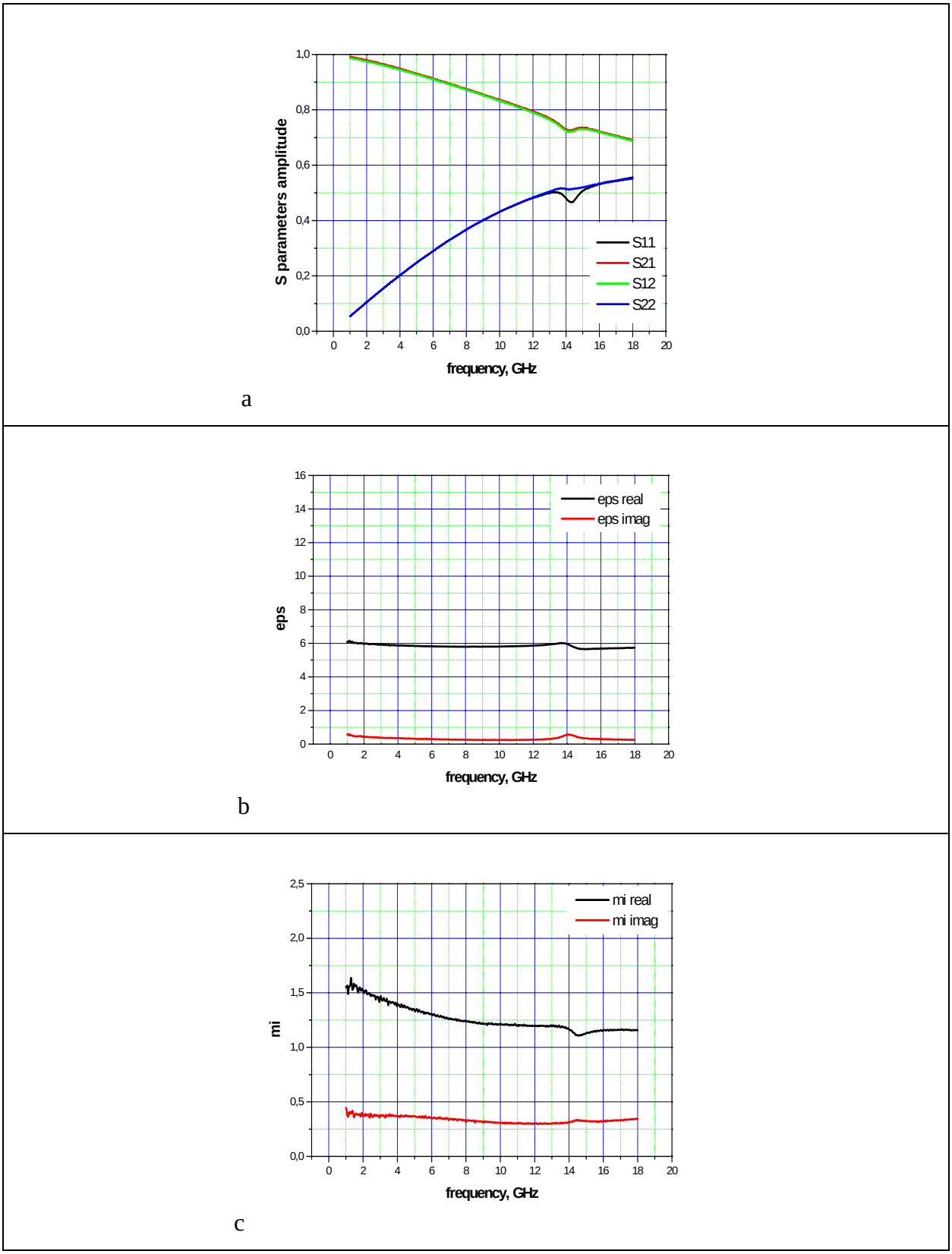

Fig. 22. Measured S-parameters and retrieved permittivity and permeability for sample CH90 (90 %wt Co powder in paraffin matrix annealed at 300^{o}C 5h, 1.15 mm ring thickness).

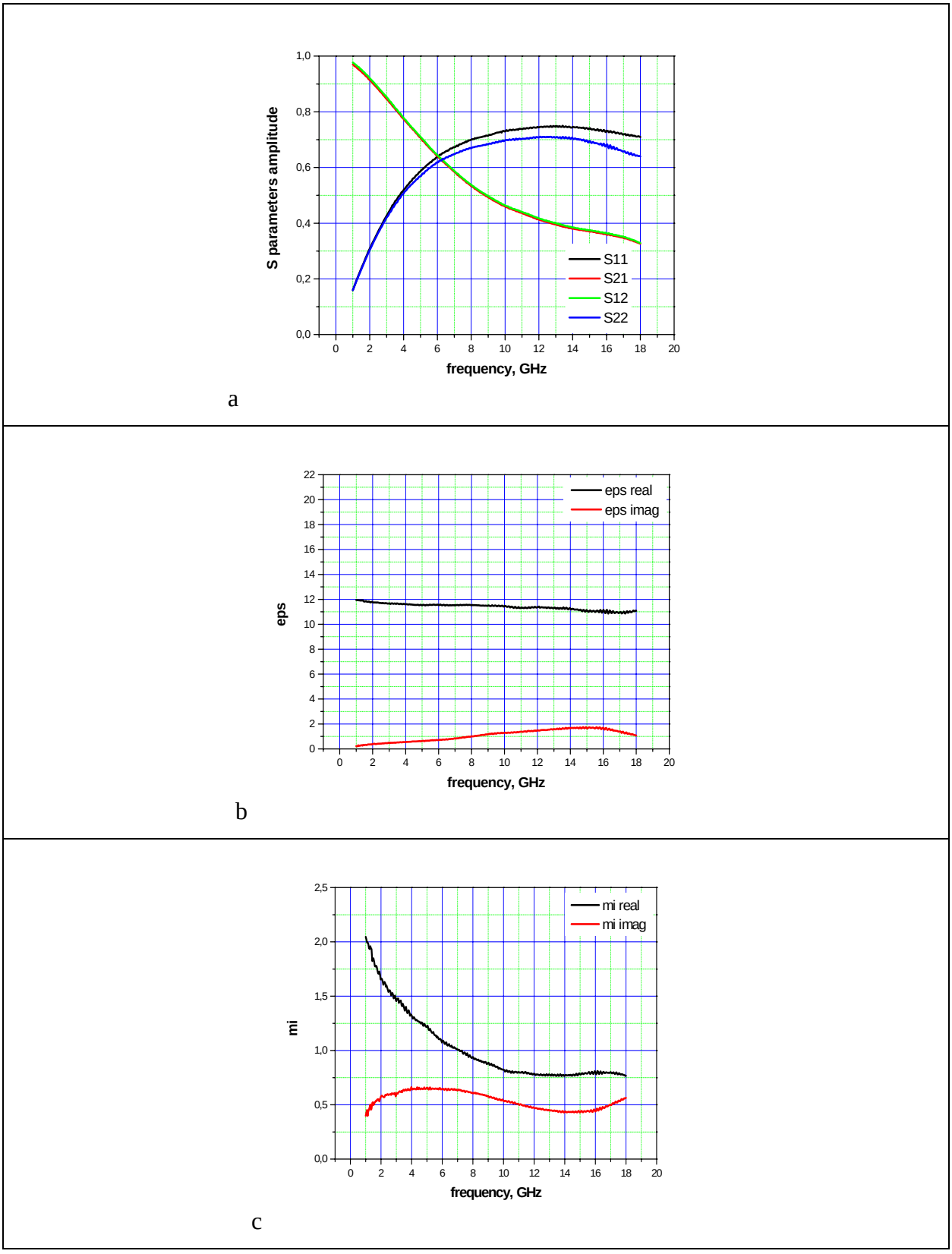

Fig. 23. Measured S-parameters and retrieved permittivity and permeability for sample NH80 (80 %wt Ni powder in paraffin matrix annealed at 300^{o}C 5h, 1.58 mm ring thickness).

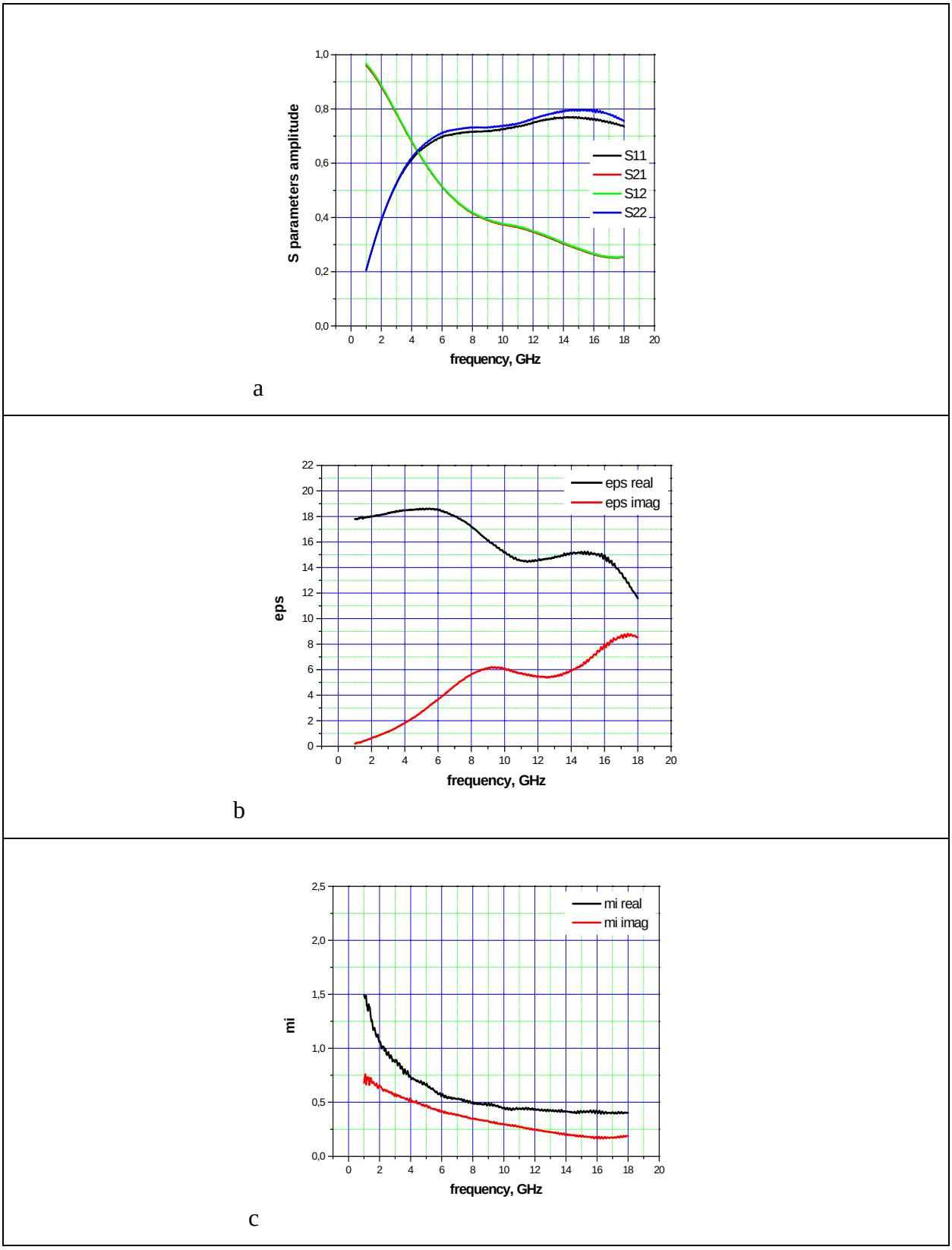

Fig. 24. Measured S-parameters and retrieved permittivity and permeability for sample NH90 (90 %wt Ni powder in paraffin matrix annealed at 300^{o}C 5h, 1.25 mm ring thickness).

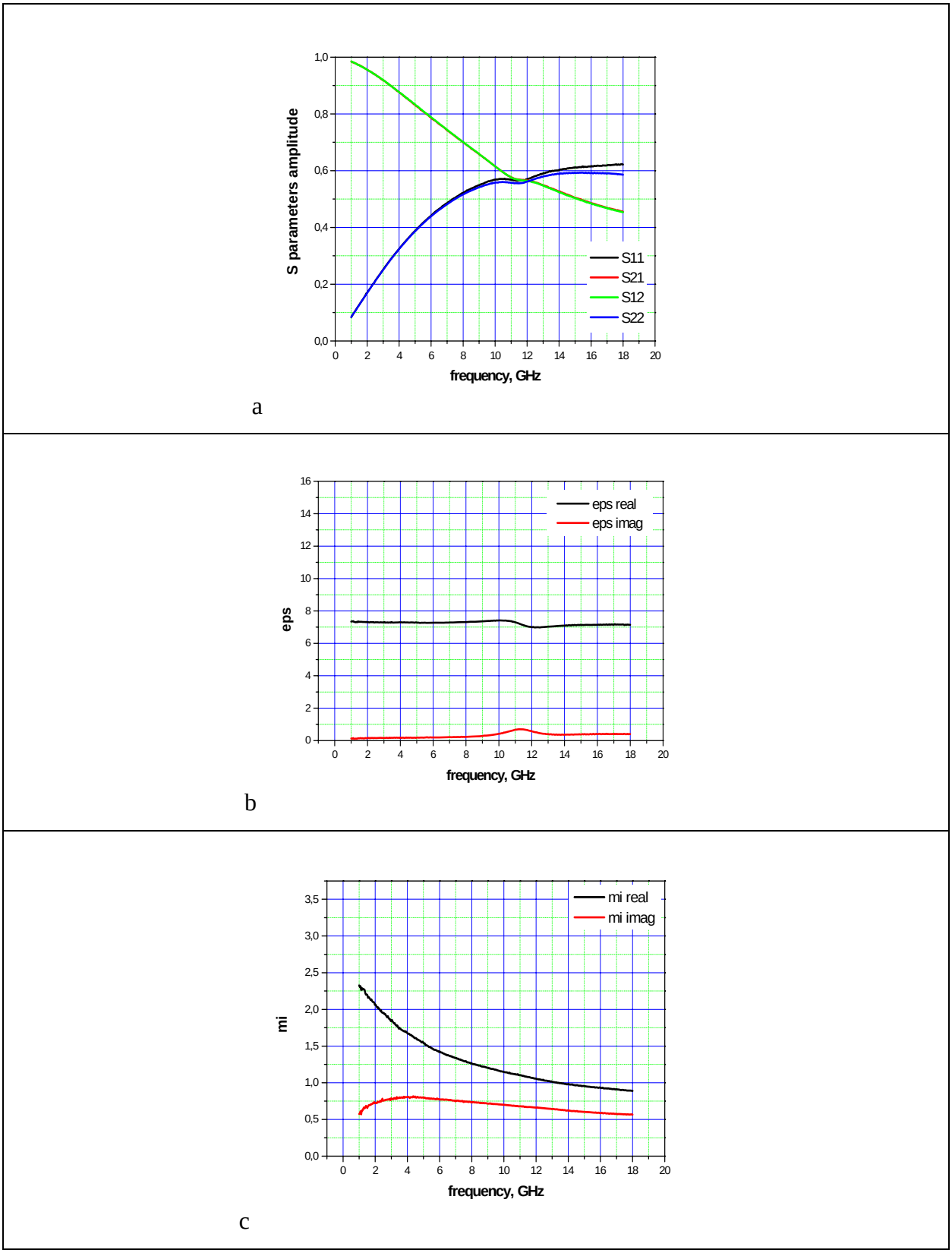

Fig. 25. Measured S-parameters and retrieved permittivity and permeability for sample FH80 (80 %wt Fe powder in paraffin matrix annealed at 300^{o}C 5h, 1.62 mm ring thickness).

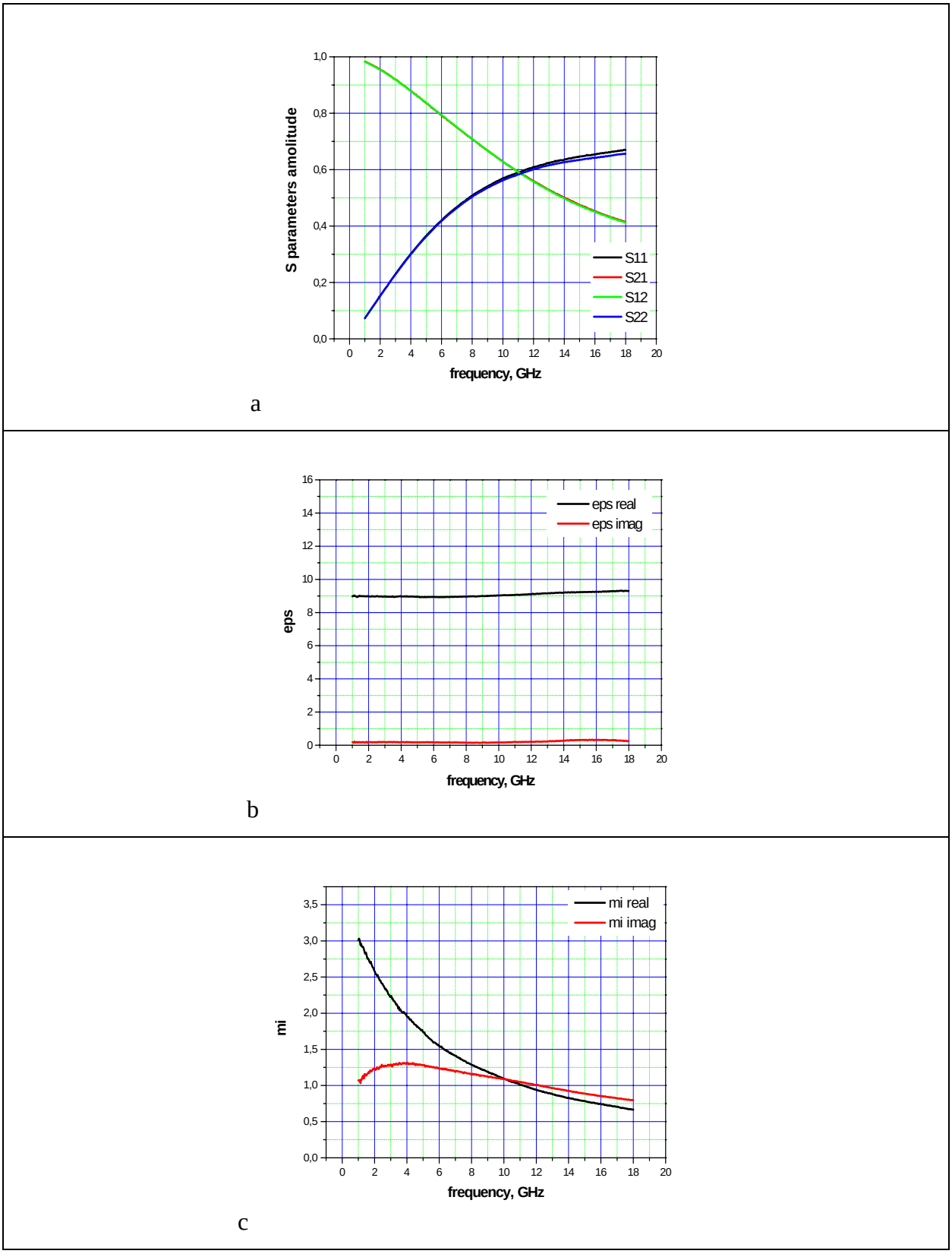

Fig. 26. Measured S-parameters and retrieved permittivity and permeability for sample FH90 (90 %wt Fe powder in paraffin matrix annealed at 300^{o}C 5h, 1.18 mm ring thickness).

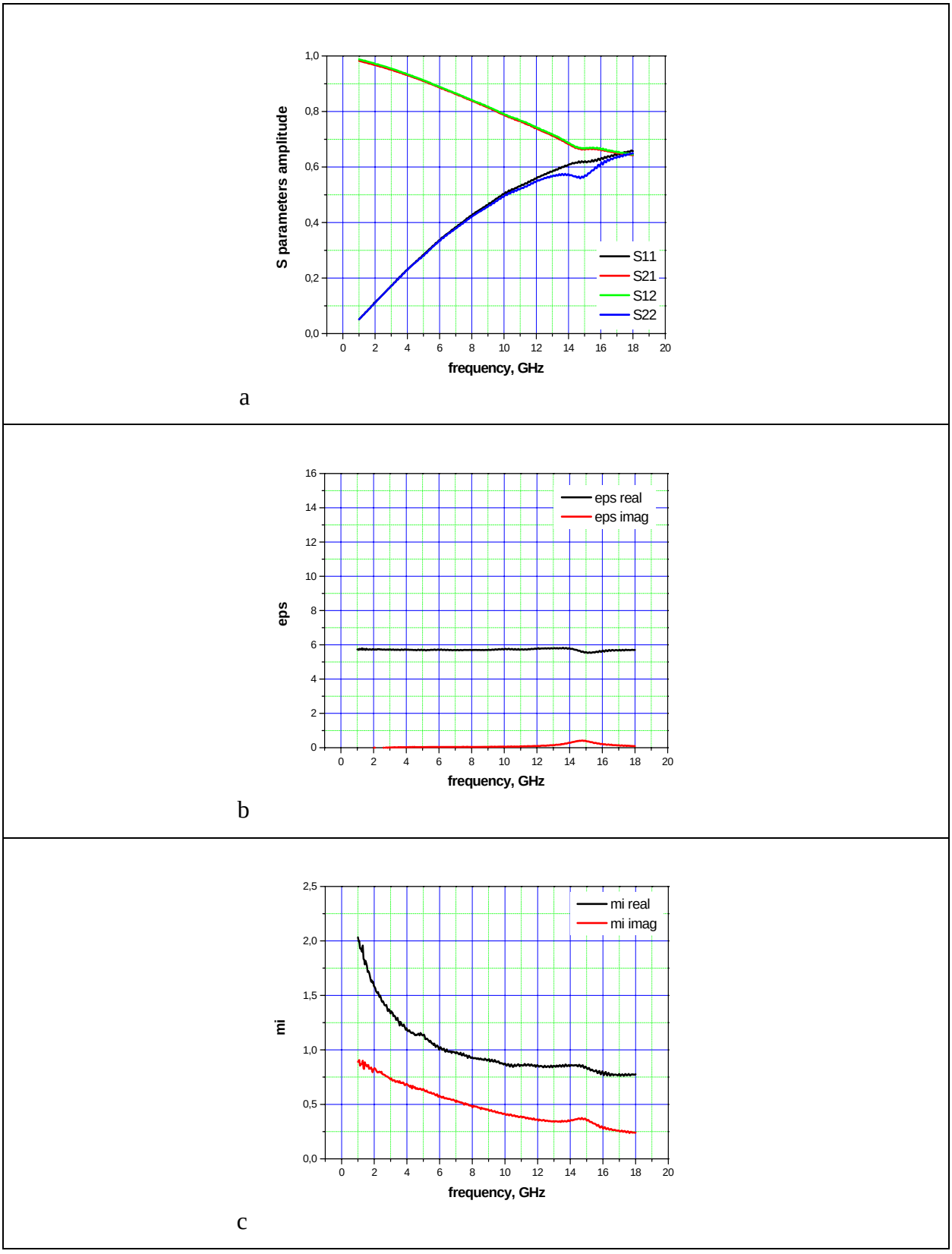

Fig. 27. Measured S-parameters and retrieved permittivity and permeability for sample FNH80 (80 %wt Fe-Co (50%-50%) powder in paraffin matrix annealed at 300^{o}C 5h, 1.30 mm ring thickness).

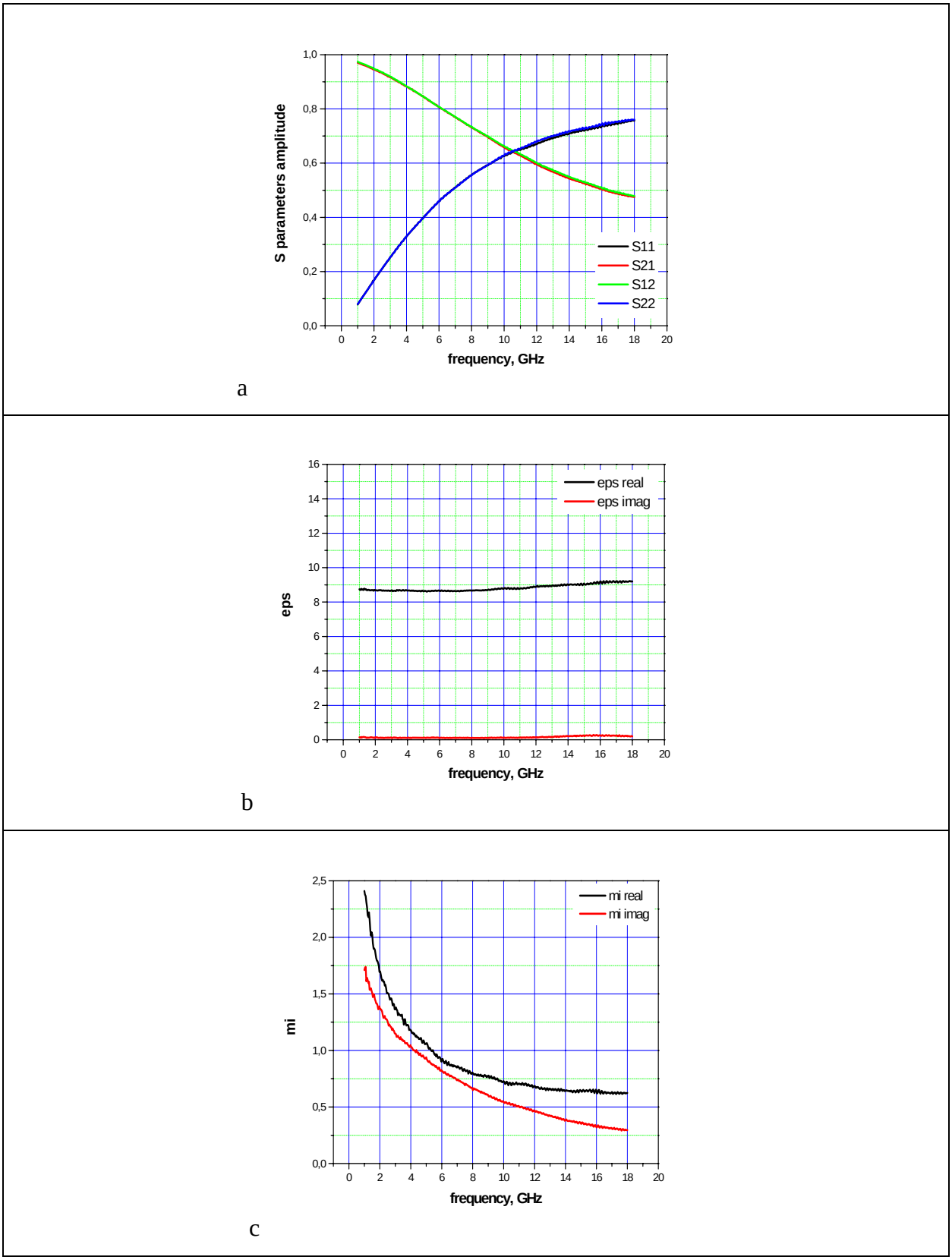

Fig. 28. Measured S-parameters and retrieved permittivity and permeability for sample FNH90 (90 %wt Fe-Co (50%-50%) powder in paraffin matrix annealed at 300^{o}C 5h, 1.20 mm ring thickness).

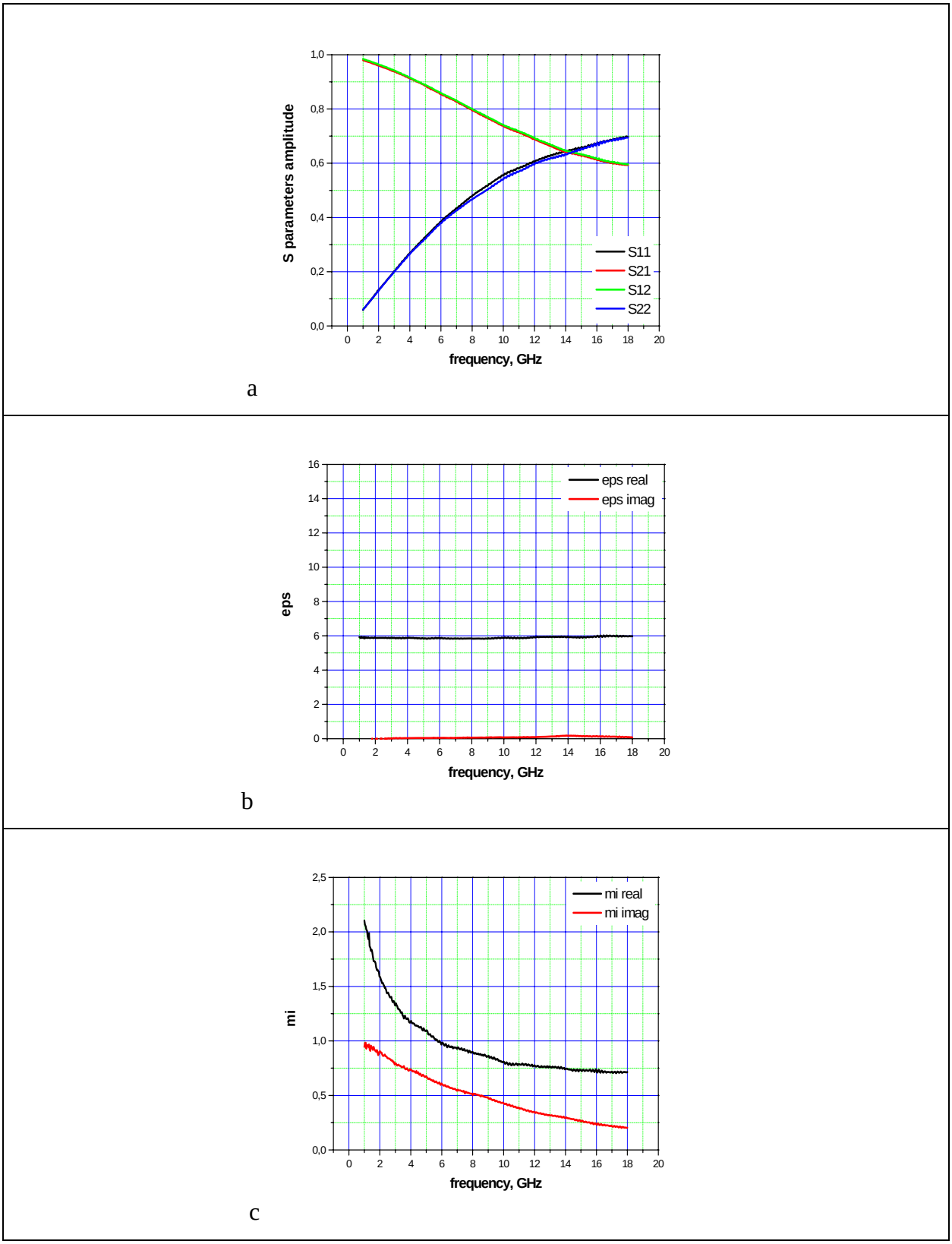

Fig. 29. Measured S-parameters and retrieved permittivity and permeability for sample FNXH80 (80 %wt Fe-Co (65%-35%) powder in paraffin matrix annealed at 300^{o}C 5h, 1.48 mm ring thickness).

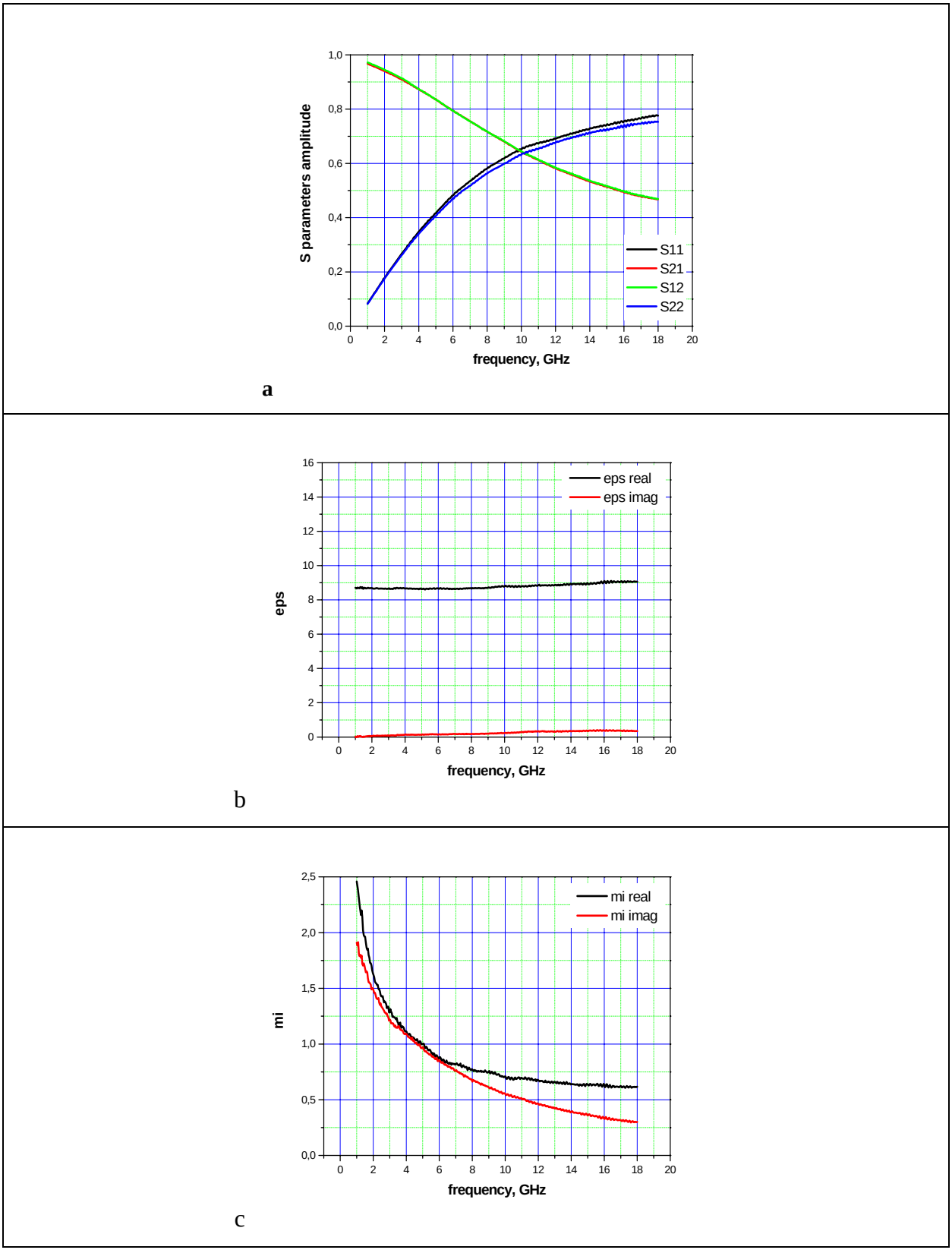

Fig. 30. Measured S-parameters and retrieved permittivity and permeability for sample FNXH90 (90 %wt Fe-Co (65%-35%) powder in paraffin matrix annealed at 300^{o}C 5h, 1.24 mm ring thickness).

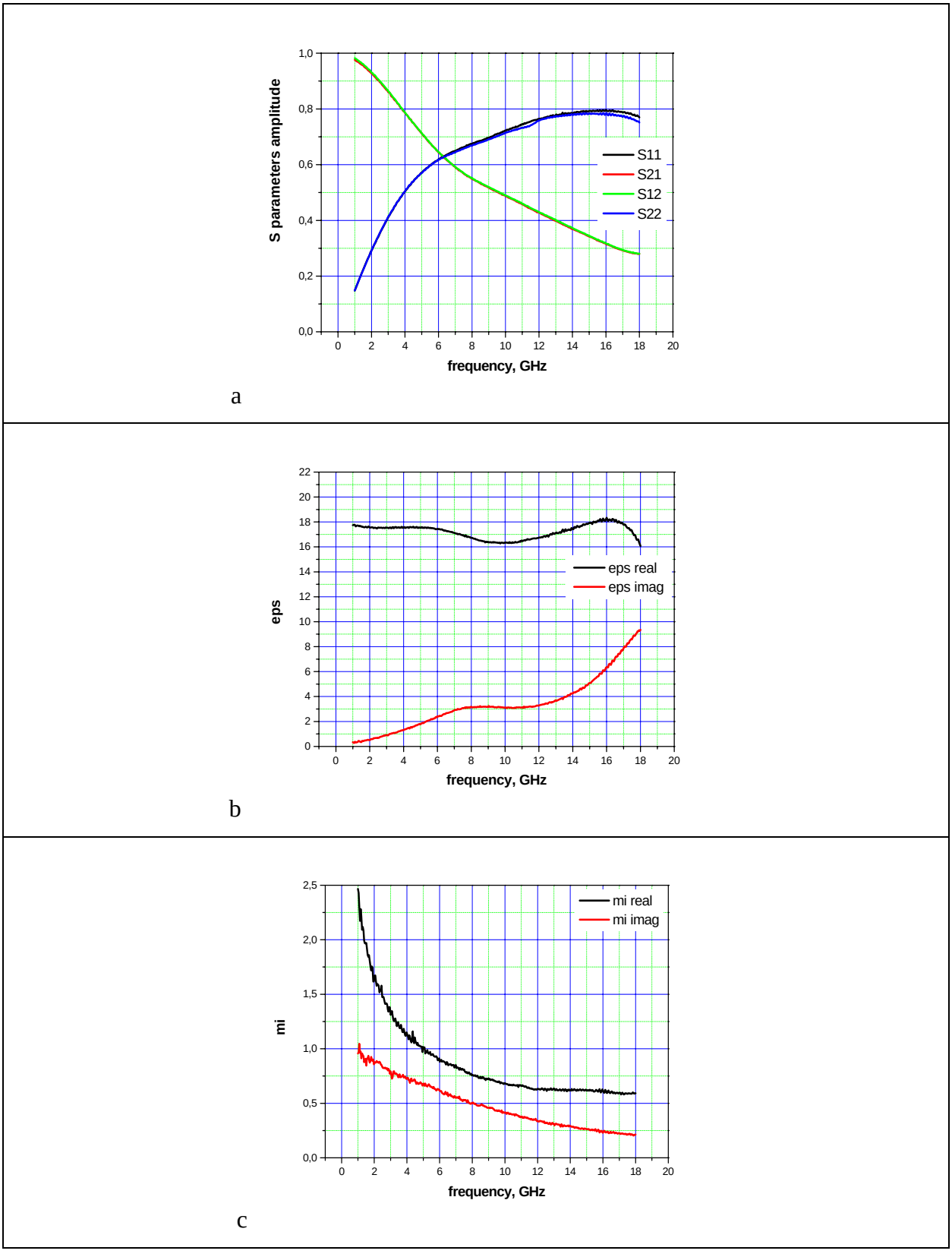

Fig. 31. Measured S-parameters and retrieved permittivity and permeability for sample NH490-3 (90 %wt Ni powder in paraffin matrix annealed at 400^{o}C 3h, 0.95 mm ring thickness).

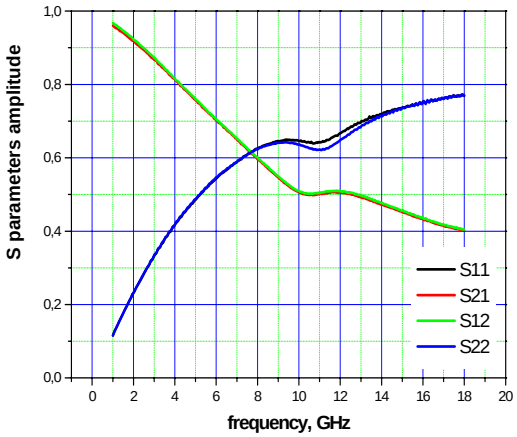

a

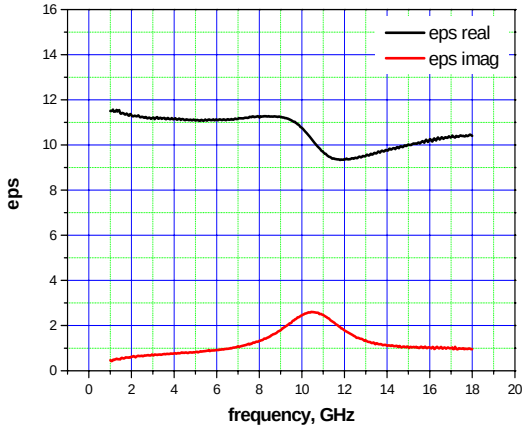

b

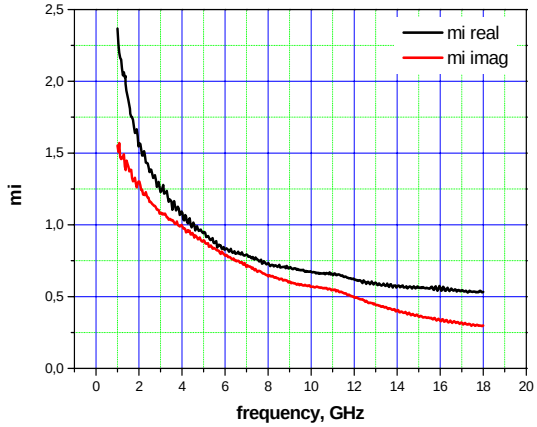

c

Fig. 32. Measured S-parameters and retrieved permittivity and permeability for sample FNH490-3 (90 %wt Fe-Ni (50%-50%) powder in paraffin matrix annealed at 400^{o}C 3h, 1,24 mm ring thickness).

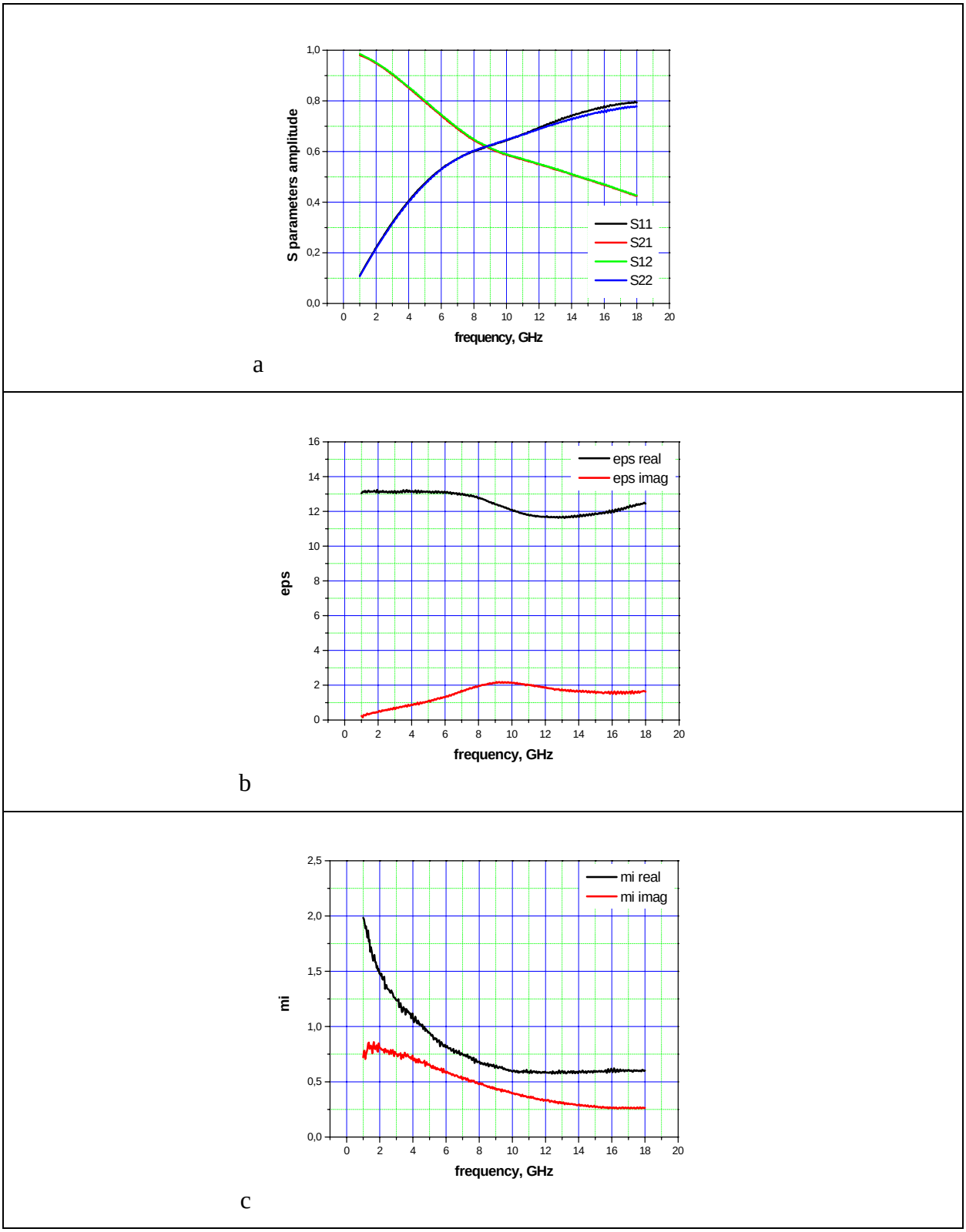

Fig. 33. Measured S-parameters and retrieved permittivity and permeability for sample NH490-6 (90 %wt Fe-Ni (50%-50%) powder in paraffin matrix annealed at 400^{o}C 6h, 1,24 mm ring thickness).

5. Discussion of the results and tasks for further research.

The idea of the usage of high particle content composites with heat-treated single metal and permalloy particles was taken from the literature [8, 9]. The short description of the permeability behavior with appearing of negative values near natural resonance frequency of the composites was given in the Chapter 3 above.

The description of the purchased powders as well as of the prepared samples is given in the beginning of Chapter 4 at the page 19. The measurement results for the powders before and after annealing are presented in Chapters 4.1 and 4.2, correspondingly. The temperature conditions were chosen according to the results of the papers [8, 9] where negative behavior of permeability was observed. The powders were annealed at 300^{o}C for 5 hours, Also, the annealing at 400^{o}C for 3 and 6 hour for some powders was attempted.

We used thin samples with thickness less or about 1.5 mm with the aim to avoid dimensional ($\lambda/2$) resonance that could add false resonance peaks in permittivity and permeability spectra.

At the Figs. 5-33 a, all four measured S-parameters are shown. This is in order to show that the prepared samples were relatively homogeneous. The transmission amplitudes in forward and reverse directions represented by S_{21} and S_{12} parameters' amplitudes are identical. The reflection amplitudes S_{11} and S_{22} in some samples appear slightly different. Probably, this is due to the no uniform intermixture of the powders at the preparation stage.

The permittivity and permeability values shown at Figs 5-33 b and Figs. 5-33 c, correspondingly, were retrieved from the S_{22} and S_{12} pair of parameters.

The measured frequency range is extended from 1 GHz to 18 GHz.

For powders without annealing, the real part of permittivity is preserved constant in the whole frequency range except for Ni powders with 80, 90% wt content (Figs. 10 b and 11 b) that exhibit relaxation type resonance at some frequencies. Its absolute values increase with the increase of the powder content. The imaginary part of permittivity is zero or takes a small non-zero value with the increase of powder content for Co, Fe and for permalloy powders. The largest dielectric losses are observed in Co powders with 90% wt content (Fig. 8 b). The imaginary part of permittivity for Ni powders is non-zero for all prepared contents beginning from the smallest one of 60 % wt (Fig. 9 b). The losses increase with the increase of the

powder content (Fig. 10 b) and exhibit resonance peaks for 80% and 90% wt content (Fig.11 b and Fig.12 b).

The increase of the imaginary part of permittivity with the increase of the powder content is related to the increase of the Ohmic contacts between the particles and consequently to increase of conductivity of the composites when the percolation threshold is still not overdrawn. The relaxation behavior observed in the nickel powders is not fully understandable. Probably, it can be assigned to creation of clusters in these samples or to the Ohmic contacts between the particles when the percolation threshold is exceeded.

The real part of the permeability for all the powders before annealing decreases with the increase of frequency. Its absolute value at the smallest measured frequency 1 GHz increases and decreases at the largest measured frequency 18 GHz falling down to the values less then 1 with the increase of the particle content for all powders except for the Ni powders. For the latter ones, the absolute value of the permeability at the beginning of the measured frequency range decreases with the increase of the particle content too. The smallest value of ~ 0.4 for the real part of permeability is achieved at the end of the measured frequency range for nickel powders (Fig. 12 c)

The imaginary part of permeability behaves in the following way. It receives small values and is preserved practically constant in the whole frequency range for small powder contents or monotonously falls down with the increase of frequency for higher contents depending on the measured powder. For the most powders, magnetic losses increase with the increase of the powder content in the whole frequency range. However for Ni powders (Figs. 8-12 c), imaginary part spectra practically do not change with the increase of powder content.

After annealing of the powders at 300^{o}C for 5 hours, the absolute values of the real part of permittivity in comparison with powders of the same powder content before annealing decrease for Co powders (see, for example, Fig. 7 b and Fig. 21 b) and for Fe powders (Fig. 14 b and Fig. 23 b) or preserve the same value for permalloy powders (see, for example, Fig. 20 b and Fig. 30 b). For Ni powder, the resonance behavior of 80% wt content powder disappears (Fig. 11 b and Fig. 23 b) but is preserved for 90% powder content (Fig. 12 b and Fig. 24 b). The absolute values of the imaginary part of permittivity in comparison with powders of the same powder content before annealing decrease for all samples. This behavior can be explained by oxidization of the particles and this way by improvement of the insulating properties of the composites. The decrease in absolute values of the real part of Co and Fe

composites for the same powder content can be explained by increase of the oxide fraction that has lower permittivity value. Preservation of the unchanged absolute value of the real part for permalloys can be explained with larger particle size of these powders (44 μm for pemalloys versus 1.6 μm and 10 μm for Co and Fe) and consequently with small influence of oxide addition. Also, permalloy and nickel powders, probably, have higher stability to oxidization.

As for permeability behavior of the annealed powders, it strongly depends on powder type and content. The absolute values of permeability real part for Co and Fe powders decrease at 1 GHz and increase in the end of the measured frequency range at 18 GHz to the value slightly larger then unit (Co powder) or slightly smaller then unit (Fe powder) in comparison with powders of the same powder content before annealing (e.g., Fig. 8 c and Fig. 22 c, Fig. 14 c and Fig. 24 c). The magnetic losses of the mentioned annealed powders in comparison with that before annealing decrease.

The real part of permeability in permalloys after annealing slightly increases in the beginning and in the end of the measured frequency range in comparison with powders before annealing for the same powder content. (e. g., Fig. 18 c and Fig. 28 c, Fig.20 c and Fig. 30 c). It is still smaller then unit at the end of the measured frequency range. The magnetic losses for two kinds of powders remain practically unchanged.

For Ni powders, temperature treatment leads to increase of the absolute values of the real and imaginary parts of permeability in comparison with untreated powders for 80% wt content in the whole frequency range (Fig. 11 c and Fig. 23 c). The permeability spectra for 90% wt powder content appear practically unchanged for real part and slightly increased for imaginary part (Fig.. 12 c and Fig. 24 c). So, the value 0.4 remains the lowest value of the real part of permeability achieved for Ni powders as well as for all studied powders. The changes in the temperature regimes (400^{o}C for 3 and 6 hours) did not lead to essential changes in permeability characteristics in comparison with treatment at 300^{o}C for 5 hours (Fig. 31 c and Fig. 33 c).

To conclude, the permeability behavior of the measured powders taking into account also permittivity analysis proves that Co and Fe powders partially loss their magnetic properties due to essential oxidization of the particles after annealing of the powders. The permalloys with larger particle dimensions undergo small changes of their dispersion characteristics with heat-treatment. The Ni powders have higher resistance to oxidization with temperature treatment, so that thin oxide layer on particle surface suppresses eddy current

effect and improves magnetic characteristics in high content composites. However, negative value of permeability was not achieved. The lowest measured value of permeability real part was 0.4

It should be noted that special least square fitting programs are needed to determine correct position of the domain wall and gyromagnetic spin resonance frequencies using the equations (28) and (29) (Chapter 3) in permeability spectra of the powders. However, taking into account the absolute values of permeability and its very smooth behavior, we can suppose that domain wall resonance in prepared composites takes place at 1-2 GHz and lower frequencies while spin resonance - in the middle of the measured frequency range (6-9 GHz). The spin resonance has relaxation type behavior. The reasons that can lead to transition from relaxation to resonance type and therefore possibility of the achieving negative permeability values are not fully understandable. Deeper knowledge is needed for understanding of the influence of particle size, particle size distribution as well as preparation conditions including temperature treatment.

In further investigations, smaller temperatures or smaller duration of temperature treatment can be applied to Co and Fe powders in order to achieve less oxidation of the particles. On the contrary, larger temperatures or longer temperature treatment can be applied to permalloy powders. In our opinion, these alterations in temperature treatment will help in better exploitation of magnetic properties of high content composites based on the mentioned powders in the viewpoint of receiving negative permeability values.

Also taking into account our previous results concerning barium titanate inclusions and high conductivity graphite elongated inclusions, free space experiments need to be done in order to investigate the influence of the inclusions' shape, size, orientation and periodicity on the resonance behaviour of the composites. For particles with mm dimensions, this can not be done with coaxial line technique.

Acknowledgement: We acknowledge the financial support by the Air Force Office of Scientific Research, Air Force Material Command, USAF, under grant number FA8655-07-1-3039.

REFERENCES

1. D. K. Rytting. Improved RF hardware and calibration methods for Network Analyzer. HP Product.
2. V. G. Gelnovatch. A computer program for the direct calibration of two-port reflectometers for automated microwave measurements. IEEE Trans.MTT, 24 (1976) 45-47.
3. R. A.. Ginley. Line-reflect-match calibration technique for the dual six-port automatic Network Analyzer. IEEE Trans. Instrum. Meas., 46 (1997) 523-526.
4. S. Rehnmark. On the calibration process of automatic Network Analyzer systems. IEEE Trans. MTT, 22 (1974) 457-458.
5. W. Kruupa, K. F. Sodomsky. An explicit solution for the scattering parameters of a linear two-port measured with an imperfect test set. IEEE Trans. MTT, 19 (1971) 122-123.
6. T. Tsutaoka, M. Hirashiba, T. Kasagi, K. Hatakeyama, K. Fujimoto. Proceedings of the Ninth International Conference on Ferrites, (2005) 663.
7. Nobuyoshi Koga, Takanori Tsutaoka. Preparation of substituted barium ferrite $BaFe_{12-x}(Ti_{0.5}Co_{0.5})_xO_{19}$ by citrate precursor method and compositional dependence of their magnetic properties. J. Magn. Magn. Mater., 313 (2007) 168–175.
8. Teruhiro Kasagi, Takanori Tsutaoka, Kenichi Hatakeyama. Negative permeability spectra in Permalloy granular composite materials. Appl. Phys. Lett., 88 (2006) 172502.
9. Teruhiro Kasagi, Shoichi Suenaga, Takanori Tsutaoka, Kenichi Hatakeyama. High frequency permeabilityof ferromagnetic metal composite materials. J. Magn. Magn. Mater., 310 (2007) 2566–2568.
10. S. T. Chui, Liangbin Hu. Theoretical investigation on the possibility of preparing left-handed materials in metallic magnetic granular composites. Phys. Rev. B, 65 (2002) 144407.
11. Takanori Tsutaoka. Frequency dispersion of complex permeability in Mn–Zn and Ni–Zn spinel ferrites and their composite materials. J. Appl. Phys., 93 (2003) 2789-2796.